

Check for updates

Carbon Neutralization



Interfacial Storage for Next-Generation Batteries: Mechanisms, Advances, and Challenges

Hui Xu¹ | Daijie Zhang¹ | Weijuan Wang² | Genxi Yu³ | Maiyong Zhu¹ D | Yunjian Liu¹

¹School of Material Science and Engineering, Jiangsu University, Zhenjiang, Jiangsu, China | ²Department of Aeronautical and Aviation Engineering, The Hong Kong Polytechnic University, Hung Hom, Kowloon, Hong Kong SAR, China | ³School of Automotive Engineering, Changzhou Institute of Technology, Changzhou, China

Correspondence: Maiyong Zhu (maiyongzhu@ujs.edu.cn) | Yunjian Liu (lyjian122331@163.com)

Received: 26 April 2025 | Revised: 21 June 2025 | Accepted: 28 June 2025

Funding: This study was supported by the Natural Science Foundation of Jiangsu Province (BK20200899) and the China Postdoctoral Science Foundation (2020M681502).

Keywords: batteries | interfacial storage | job-sharing | solid-state electrolytes | space charge regions

ABSTRACT

Modern battery systems confront inherent kinetic and durability limitations due to the simultaneous accommodation of electrons and ions within the bulk phase of electrode materials. A paradigm-shifting strategy, inspired by the "job-sharing" electrochemistry concept, addresses these challenges by decoupling electron and ion storage into distinct space charge regions at engineered heterointerfaces. Despite the considerable promise of interfacial storage mechanisms in advancing next-generation batteries, the field lacks a coherent theoretical framework and universal design principles to fully harness their potential across diverse material systems and device architectures. This review provides a fundamental understanding of interfacial storage mechanisms while elucidating their impacts on electrochemical performance. We critically analyze recent breakthroughs in nanocomposite/heterostructure electrodes and solid-state electrolytes, highlighting how rational interface engineering can enhance charge transfer kinetics, transcend intrinsic bulk storage limitations, improve structural stability, and mitigate space charge effects at electrode/electrolyte interfaces. Moreover, we discuss cutting-edge characterization methodologies essential for probing interfacial evolution and charge storage behavior. Finally, we identify pivotal challenges in interfacial stability control and scalable manufacturing, while proposing promising research directions, such as atomic-scale interface engineering and sustainable fabrication strategies, to advance carbon-neutral energy storage systems through innovative electrochemical approaches.

1 | Introduction

The reduction of carbon emissions and the achievement of carbon neutrality are widely recognized as critical missions for current society [1–3]. In pursuit of these objectives, the integration of renewable energy systems has undergone rapid development, offering effective solutions to both the ongoing energy crisis and pressing environmental issues [4, 5]. However, effective implementation of grid-connected renewable energy requires electrochemical energy storage (EES) systems with superior

performance [6–9]. While lithium-ion batteries (LIBs) dominate EES applications, emerging technologies such as sodium-ion batteries (SIBs) and aqueous zinc-ion batteries (AZIBs) are positioned to play key roles in future energy infrastructure [10, 11]. These systems rely fundamentally on ion/electron intercalation mechanisms within crystalline electrode frameworks. In ionic compounds, this process typically involves ion intercalation into interstitial or vacant lattice sites, accompanied by electron transfer that reduces transition metal cations to lower oxidation states [12–14]. Although bulk storage enables theoretically high

This is an open access article under the terms of the Creative Commons Attribution License, which permits use, distribution and reproduction in any medium, provided the original work is properly cited.

© 2025 The Author(s). Carbon Neutralization published by Wenzhou University and John Wiley & Sons Australia, Ltd.

capacities, it is intrinsically limited by sluggish solid-state diffusion kinetics [15]. Moreover, the cohabitation of ions and electrons in identical crystalline phases imposes stringent requirements on the structural flexibility and redox stability of electrode materials, potentially resulting in structural degradation and consequent capacity fading during cycling.

An innovative strategy in addressing these limitations involves the decoupling of ion and electron storage through tailored nanocomposites/heterostructures with spatially segregated charge reservoirs. This charge storage mechanism, initially conceptualized as "job-sharing" electrochemistry by Maier et al. [16], enables discrete charge carrier accommodation in distinct space charge regions at two-phase interfaces (Figure 1a), despite constituent phases lacking individual charge storage capability. Notably, this interfacial storage phenomenon is not restricted to advanced material systems but is fundamentally intrinsic to heterogeneous systems, manifesting across diverse interfaces

including phase boundaries in composites, electrode/current collector interfaces, and electrode/electrolyte interfaces [19]. The principal advantage of interfacial storage lies in its enhanced kinetics, which arise from segregated transport pathways for ionic and electronic carriers. This stands in marked contrast to conventional bulk storage mechanisms (Figure 1b), in which coupled ion-electron transport through single-phase systems imposes kinetic limitations, as the material must simultaneously accommodate both charge carriers while maintaining high electronic and ionic conductivities to achieve a high power density. A successful demonstration of interfacial storage for kinetics enhancement is the RbAg₄I₅-graphite composite, which demonstrates ultrafast chemical diffusion coefficients ($\sim 5.0 \times 10^{-4} \, {\rm cm}^2 \, {\rm s}^{-1}$) (Figure 1c), surpassing even aqueous solutions of sodium chloride [17].

Interfacial storage represents a rapid reaction mechanism that is distinct from surface capacitive processes, although both are

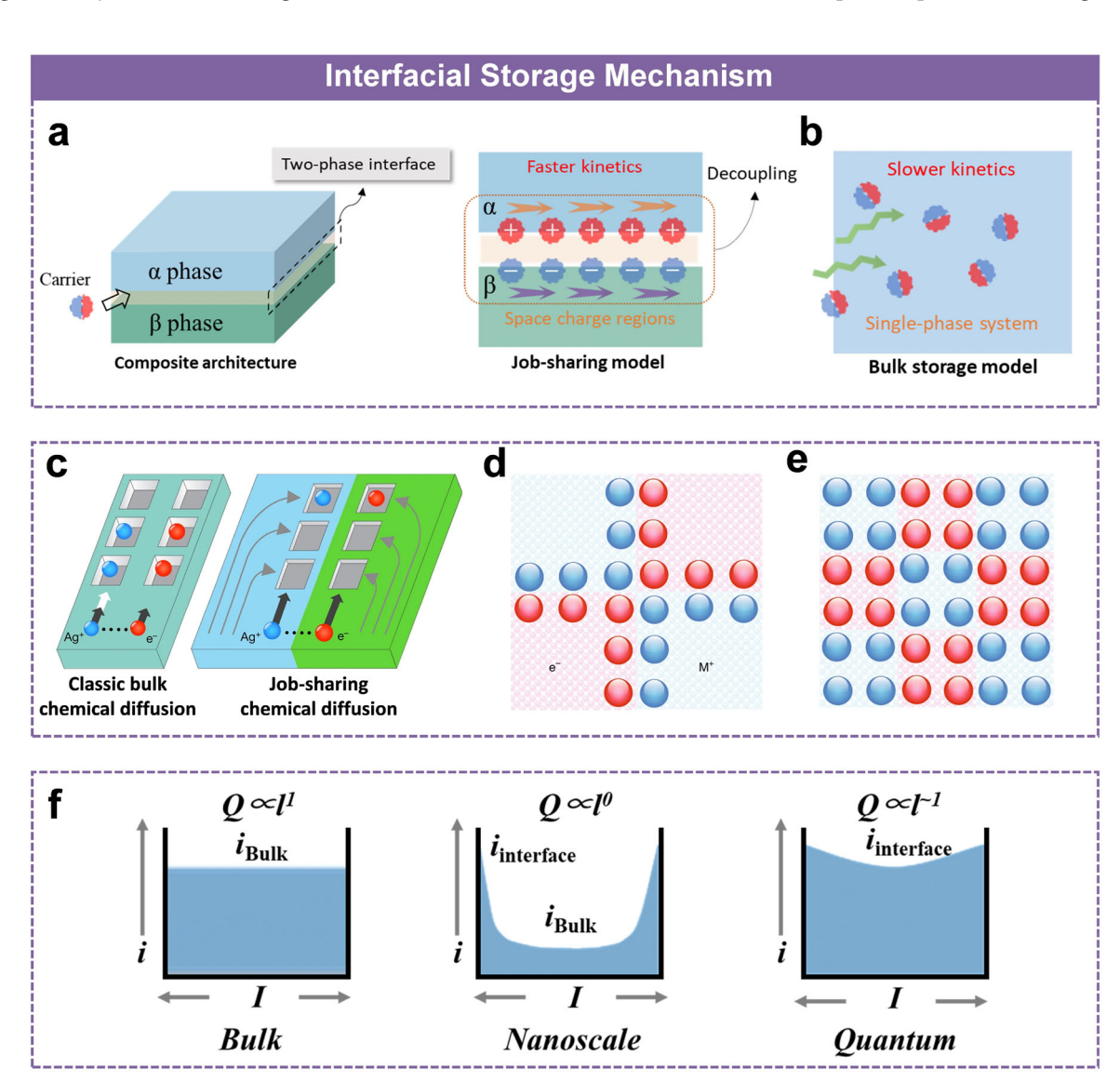


FIGURE 1 | Schematic of (a) interfacial storage and (b) bulk storage mechanisms. (c) Schematic of bulk and interfacial diffusion pathways [17]. Reproduced with permission: Copyright 2016, Springer. (d) Schematic of interfacial storage in micron or submicron-scale materials, where the blue balls represent metal ions (e.g., Li⁺ or Na⁺) and the red ones represent electrons. (e) Schematic of interface-dominated storage in dimensionally optimized nanocomposites [16]. Reproduced with permission: Copyright 2018, Springer. (f) Schematic of the thickness (*l*)-capacity (*Q*) relationship (adapted with permission from Ref. [18]). Reproduced with permission: Copyright 2013, WILEY-VCH.

classified under capacitive behavior. The key distinction lies in the spatial distribution and nature of charge storage. In the surface capacitive processes, charge storage occurs strictly at or near the material's surface, with storage capacity being directly proportional to the available surface area. In contrast, interfacial storage involves rapid ion intercalation/deintercalation into the interfacial regions of composites or heterostructures, resulting in a capacity that is primarily determined by interfacial density rather than surface area. Benefiting from inherent capacitive characteristics, interfacial storage exhibits both superior kinetics and remarkable cycling stability. This enhanced cyclability originates from three key advantages: First, unlike conventional bulk storage mechanisms, interfacial processes avoid solid-phase diffusion, thus preventing phase transitions that typically cause structural degradation. Second, at engineered heterointerfaces, controlled lattice mismatch is harnessed to form specific defect structures, which act as strain buffers, effectively mitigating interfacial strain and significantly reducing mechanical stress during repeated cycling. Third, the reversible breakage/reconstruction of interfacial heterogeneous bonds during charge/discharge processes enables intrinsic selfhealing properties, thereby maintaining electrode structural integrity over extended operation. These synergistic effects collectively ensure exceptional long-term stability of interfacial storage systems, even when operated under high-rate conditions.

Beyond offering kinetic and cyclability advantages, interfacial storage mechanisms also hold significant potential for capacity enhancement by extending the effective charge storage domains. Since interfacial storage is primarily confined to space charge regions at interfaces [20], achieving high storage capacities requires maximized interfacial density through atomic-scale interface engineering. However, conventional electrode materials with micron or submicron-scale structures show intrinsically limited interfacial-to-bulk volume ratios, rendering interfacial storage contributions negligible at macroscopic scales (Figure 1d) [16]. In contrast, dimensionally optimized nanocomposites undergo a fundamental inversion of this paradigm, where interfacial and bulk phases achieve size commensurability (Figure 1e) [16]. This optimization enables interfacial storage to evolve from a supplementary role to the dominant contributor to battery capacity.

This paradigm shift establishes thickness-dependent scaling laws as the governing principle for electrochemical performance. Maier' group has provided a comprehensive analysis of this phenomenon, and interested readers are directed to their detailed studies [18, 21]. Within this framework, three distinct operational regimes emerge (Figure 1f): (i) Bulk-dominant regime: Conventional volumetric scaling $(Q \propto l^1)$ prevails, governed by Faradaic processes with bulk diffusion limitations. In this size range, particle size reduction exhibits a negligible effect on capacity due to persistent rate limitation by ion transport. The electrochemical response remains dominated by traditional intercalation dynamics where complete particle utilization can be achieved through bulk diffusion processes; (ii) Transitional nanoscale regime: The stored capacity exhibits size-independent behavior $(Q \propto l^0)$. As particle sizes shrink into the nanoscale, space charge regions partially penetrate the particle but fail to fully span its volume. This creates a dual storage mechanism where residual bulk diffusion in the particle

core competes with interfacial processes. The reduced bulk contribution is counterbalanced by the increased interfacial contribution, resulting in a net capacity that remains independent of particle size; (iii) Quantum-confined regime: Capacity again displays a thickness dependence $(Q \propto l^{-1})$ due to complete overlap of space charge regions. Below a critical particle size threshold, interfacial storage becomes the dominant mechanism, and quantum confinement effects facilitate full overlap of charge storage regions, rendering capacity directly proportional to particle thickness. The transition from bulk-dominated to interface-governed storage mechanisms overcomes conventional energy storage limitations by utilizing atomically engineered heterointerfaces as the critical enabler for mitigating the tradeoffs between energy density and power density.

The recognition of interfacial storage as a triple-enabler for kinetic acceleration, cycle stability improvement, and capacity enhancement is paramount in developing next-generation batteries that simultaneously achieve high-energy storage, ultrafast charge transfer, and long-term cycling characteristics. Despite its significant potential, this design paradigm remains underexplored in current research. Existing reviews on interfacial storage lack a coherent theoretical framework and universal design principles, limiting their ability to fully leverage the advantages across diverse material systems and device architectures. In contrast to these previous works, this review bridges this knowledge gap by clarifying the fundamental principles of interfacial storage mechanisms and their multifaceted impacts on electrochemical performance. Through a comprehensive summary and systematic analysis of recent advances in nanocomposite/heterostructure electrodes and solid-state electrolytes, we demonstrate how rational interface engineering can accelerate charge transfer kinetics, overcome intrinsic bulk storage constraints, enhance structural stability, and suppress space charge effects at electrode/electrolyte interfaces. Building on these insights, we establish a unified framework that elucidates complex interfacial phenomena in modern battery systems, offering design principles to optimize electrochemical performance. To guide future research, we outline crucial characterization methodologies essential for probing interfacial structure evolution and charge storage behavior at atomic to mesoscopic scales. Finally, this review concludes with a critical analysis of current challenges and forward-looking perspectives on the most promising research directions in the interfacial storage field.

2 | Fundamental Principles of Interfacial Storage

Interfacial storage is governed by the formation and modulation of space charge regions at heterointerfaces, where different materials meet, creating localized regions of charge redistribution [22, 23]. When two materials with differing electronic or ionic properties form an interface, such as a semiconductor coupled with a conductor, or two oxides with distinct band structures, their inherent differences in Fermi levels or chemical potentials drive charge transfer across the boundary [24]. Electrons migrate from the material with a lower work function to the one with a higher work function until equilibrium is achieved, establishing a built-in electric field across the interface [25]. This field polarizes the adjacent regions, depleting or

accumulating charge carriers in a spatial domain known as the space charge regions, typically confined to dimensions comparable to the Debye screening length (1-10 nm) [18]. Within this nanoscale zone, ions are electrostatically adsorbed at interfacial sites, while electrons are confined to energy states aligned with the interfacial electric potential. The decoupling of charge carriers in the space charge regions bypasses the need for deep bulk diffusion, enabling rapid ion diffusion and electron transfer. Moreover, the built-in electric field not only stabilizes the charge separation but also lowers activation energy barriers for interfacial reactions, accelerating kinetics by orders of magnitude compared to diffusion-limited processes. This synergetic interplay of charge redistribution, fielddriven ion migration, and quantum mechanical effects (e.g., electron tunneling across ultrathin interfaces) forms the foundation of interfacial storage, where charge is stored not within bulk lattice sites but in the nanoscale space charge regions of the heterointerface.

Beyond charge redistribution, the built-in electric field governs both thermodynamic stability and kinetic behavior during interfacial storage processes. Thermodynamically, it establishes a potential gradient that dictates the equilibrium distribution of ions and electrons at the heterointerface [26]. For instance, in a heterostructure composed of an ion conductor and an electron conductor, this field aligns the ion and electron energy levels, creating preferential adsorption sites for ions (e.g., Li⁺, Na⁺) at interfacial defects or vacancies. This alignment modulates the effective redox potential of the storage process, enabling higher operational voltages or capacities compared to bulk materials. Kinetically, the field acts as an electrostatic "pump," driving ions toward the interface while simultaneously funneling electrons through low-resistance pathways, effectively accelerating ion and electron transport [27]. This decoupling eliminates the cross-talk between slow ion diffusion and resistive electron transfer that plagues bulk materials, allowing interfacial storage to achieve ultrafast charge/discharge rates. Moreover, the confinement of space charge regions ensures that ion migration occurs over atomic-scale distances [28, 29], thereby bypassing the sluggish solid-state diffusion inherent to conventional intercalation mechanisms.

The practical implementation of interfacial storage requires precise control over space charge regions, as their instability directly influences device performance. Excessive interfacial charge density can lead to electrostatic screening effects, where the built-in electric field is weakened through counterion accumulation, reducing storage efficiency. Similarly, mechanical strain arising from lattice mismatch at interfaces may distort the space charge regions, altering the local electric field and aggravating cycling stability [30, 31]. To mitigate these challenges, atomic-scale interface engineering is essential. For example, tailoring the defect structure [32, 33] or introducing gradient compositions [34] at heterointerfaces can homogenize the built-in electric field, ensuring uniform charge distribution. Additionally, designing heterointerfaces with self-regulating charge compensation mechanisms, such as redox-active surface groups or dynamically adaptive space charge regions, could maintain field stability during cycling [35]. These design principles highlight the delicate balance required to harness interfacial storage, where optimizing the spatial and energetic landscape of space charge regions to maximize charge storage capacity while preserving the integrity of the built-in electric field. When achieved, interfacial storage unlocks unprecedented performance, merging high energy density with ultrafast kinetics, and redefining the limits of modern battery systems.

3 | Interface Engineering in Modern Battery Systems

Recent breakthroughs in nanocomposites/heterostructures have enabled precise control over interfacial density at the nanoscale, spurring considerable research efforts to explore interfacial phenomena in battery systems. Although interfacial functionalities exhibit system-dependent variations, substantial experimental evidence exhibits that rational interface engineering act as a universal performance optimization strategy. This section systematically examines recent advances in nanocomposite/heterostructure electrodes and solid-state electrolytes, highlighting how rational interface engineering can (i) enhance charge transfer kinetics, (ii) overcome intrinsic bulk storage limitations, (iii) reinforce electrode structural stability, and (iv) suppress space charge effects at electrode/electrolyte interfaces, as illuminated in Figure 2.

3.1 | Acceleration of Charge Transfer Kinetics

Interfacial storage profoundly influences charge transfer kinetics by decoupling ion and electron transport pathways. In bulk materials,

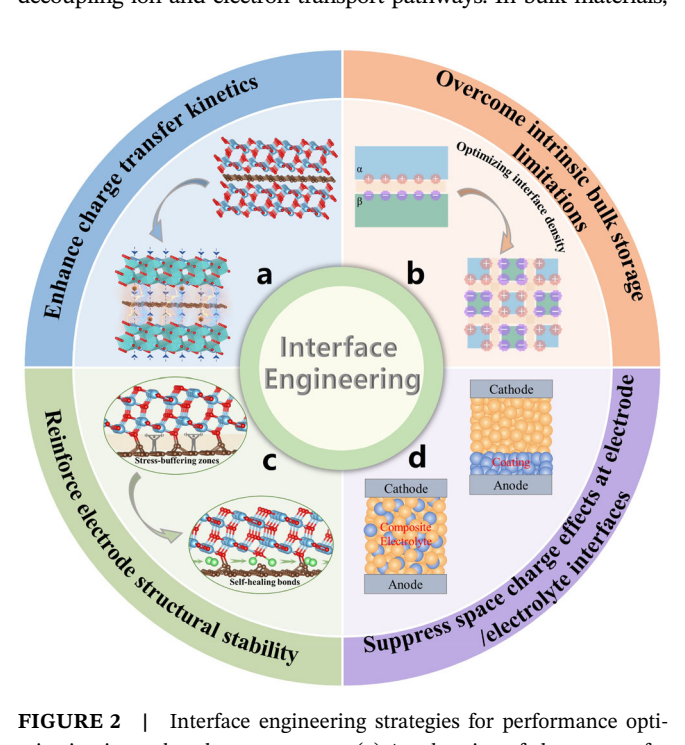


FIGURE 2 | Interface engineering strategies for performance optimization in modern battery systems. (a) Acceleration of charge transfer kinetics through built-in electric field and tailored heterointerfaces, (b) expansion of storage capacity beyond bulk limitations by optimizing interface density to enhance interface storage contribution, (c) reinforcement of structural stability via stress-buffering interphases and self-healing bonds, and (d) suppression of space-charge effect through composite electrolyte design and functional interfacial coatings.

sluggish ion diffusion often limits rate performance, particularly in intercalation hosts like graphite [36] or transition metal oxides [37]. At heterointerfaces, however, the spatial separation of ion adsorption sites and electronic conduction pathways minimizes cross-talk between ionic and electronic resistances. The resulting charge redistribution induces localized space charge regions with intrinsic built-in electric fields, synergistically lowering migration barriers while amplifying carrier flux. As exemplified in Table 1, these engineered heterostructures demonstrate remarkable advancements in charge transfer kinetics and electrochemical performance across diverse battery systems.

Zheng et al. [38] developed ultrathin Bi₂MoO₆ nanosheets through a scalable wet-chemical synthesis, featuring alternating Bi₂O₂/MoO₄ layers with engineered interlayer channels and oxygen vacancies (OVs) (Figure 3a). Density functional theory (DFT) calculations revealed that this structure induces asymmetric charge distribution between interlayers and near OV sites (Figure 3b), generating localized electric fields that effectively promote Li⁺ diffusion while improving rate performance. The concomitant interfacial migration pathways further synergize to boost Li⁺ storage capacity. Fang et al. [39] constructed Sb₂S₃-SnS₂ heterostructures with "ion-reservoir" characteristics for Na⁺/Li⁺ storage. The engineered heterointerfaces establish inherent electric fields that directionally guide cation migration toward negatively charged domains (Figure 3c), substantially lowering diffusion barriers and realizing ~66% capacity retention at 50-fold increase in the current density (Figure 3d). Similarly, Yin et al. [40] designed SnO/ SnO₂ heterostructures anchored on reduced graphene oxide (rGO), creating a built-in electric field in the interfaces that shortened electron pathways and enabled multi-channel Li⁺ diffusion, as evidenced by experimental results (Figure 3e). The heterointerface-rich composite improved Li⁺ transport kinetics while achieving a high capacity of 498 mAh g⁻¹ after 400 cycles. Complementing these findings, Lu et al. [41] developed an electrostatically driven self-assembly to engineer atomic-scale interfacial electric fields in a TiNbO $_5$ /rGO heterostructure, establishing dual ion/electron transport pathways, which achieved a remarkable reversible Na $^+$ storage capacity of 245 mAh g $^{-1}$ at 0.05 A g $^{-1}$. Theoretical analysis also confirmed that the electric field enhanced the electrical conductivity and facilitated electron transfer at the atomic interface.

Liang et al. [42] designed H₂V₃O₈/MXene heterostructures via hydrothermal synthesis. DFT calculations (Figure 3f) suggest that an intrinsic electric field at the H₂V₃O₈-MXene interface is pivotal in accelerating Zn²⁺ diffusion and enhancing the structural stability at the interface, ultimately resulting in superior Zn²⁺ storage capacity of 437 mAh g⁻¹ after 500 cycles at 3 A g⁻¹. Li et al. [43] developed MoS₂/ZnS heterostructures through substrate-guided in situ self-assembly. The intrinsic built-in electric field at MoS₂/ ZnS interfaces facilitates Zn²⁺ transport, which reduces ab-plane diffusion barriers by 1.3 eV while activates c-axis ion migration pathways, achieving exceptional cycle performance with 87% capacity retention after 10,000 cycles at 10 A g⁻¹. Additionally, Xiao et al. [44] enhanced Zn²⁺ diffusion kinetics in Ba-V₆O₁₆·3H₂O/MoS₂ heterostructures. The Fermi level disparity induced a built-in electric field at the heterointerface, which drives Zn²⁺ migration toward the cathode and improving ion diffusion kinetics during discharge. Galvanostatic intermittent titration technique (GITT) and finite element analysis (FEA) quantitatively validated this field-enhanced transport mechanism, revealing a Zn^{2+} diffusion coefficient of 7.5×10^{-8} cm² s⁻¹ (Figure 3g.h). surpassing that of most reported V-based cathodes.

Beyond the intrinsic acceleration effects of built-in electric fields, rationally designed interface architectures offer additional pathways to optimize charge transport dynamics. Kim et al. [45] demonstrated that lattice distortion at the Nb_2O_5/MoO_2 heterointerfaces created expanded ionic pathways, significantly boosting K^+ diffusion in micron-scale electrodes (Figure 4a,b). This enhancement

TABLE 1 | Interface engineering strategies to enhance charge transfer kinetics.

| Material | Battery Type | SC/R | RT/CN/R | References |
|--|---------------|---------------------|--------------------|------------|
| Bi ₂ MoO ₆ | LIBs | 903/0.05 | 72%/1500/2 | [38] |
| Sb ₂ S ₃ -SnS ₂ | SIBs and LIBs | 655/0.5 and 936/0.5 | 85%/100/0.5 (LIBs) | [39] |
| SnO/SnO ₂ @rGO | LIBs | 1331/0.1 | 46%/400/1 | [40] |
| TiNbO ₅ /rGO | SIBs | 1099/0.05 | 99%/3000/1 | [41] |
| $H_2V_3O_8/MXene$ | AZIBs | 437/3 | 100%/9000/10 | [42] |
| MoS ₂ /ZnS | AZIBs | 337/0.05 | 87%/10000/10 | [43] |
| $BaV_6O_{16}{\cdot}3H_2O/MoS_2$ | AZIBs | 454/0.1 | 95%/10000/5 | [44] |
| Nb ₂ O ₅ /MoO ₂ | KIBs | 204/0.1 | 86%/1000/1 | [45] |
| MnO/MnS | LIBs | 1235/0.2 | 86%/2000/3 | [46] |
| CC@VN-MoS ₂ | AZIBs | 258/0.05 | \ | [47] |
| MnO ₂ @PANI | AZIBs | 402/0.5 | 78%/1000/2 | [48] |
| TiO ₂ /GO | LIBs | 281/0.168 | \ | [49] |
| $VSe_{2-x} \cdot nH_2O$ | AZIBs | 425/1 | 100%/5000/10 | [50] |
| $\alpha\text{-MnO}_2@\delta\text{-MnO}_2$ | AZIBs | 402/0.2 | 84%/1000/1 | [51] |
| MoS ₂ @EG | AZIBs | 166/0.2 | 100%/2500/10 | [52] |

Abbreviation: CN, cycle numbers; GO, graphene oxide; PANI, polyaniline; RT, retention; R, rate (A·g⁻¹); rGO, reduced graphene oxide; SC, specific capacity (mAh·g⁻¹).

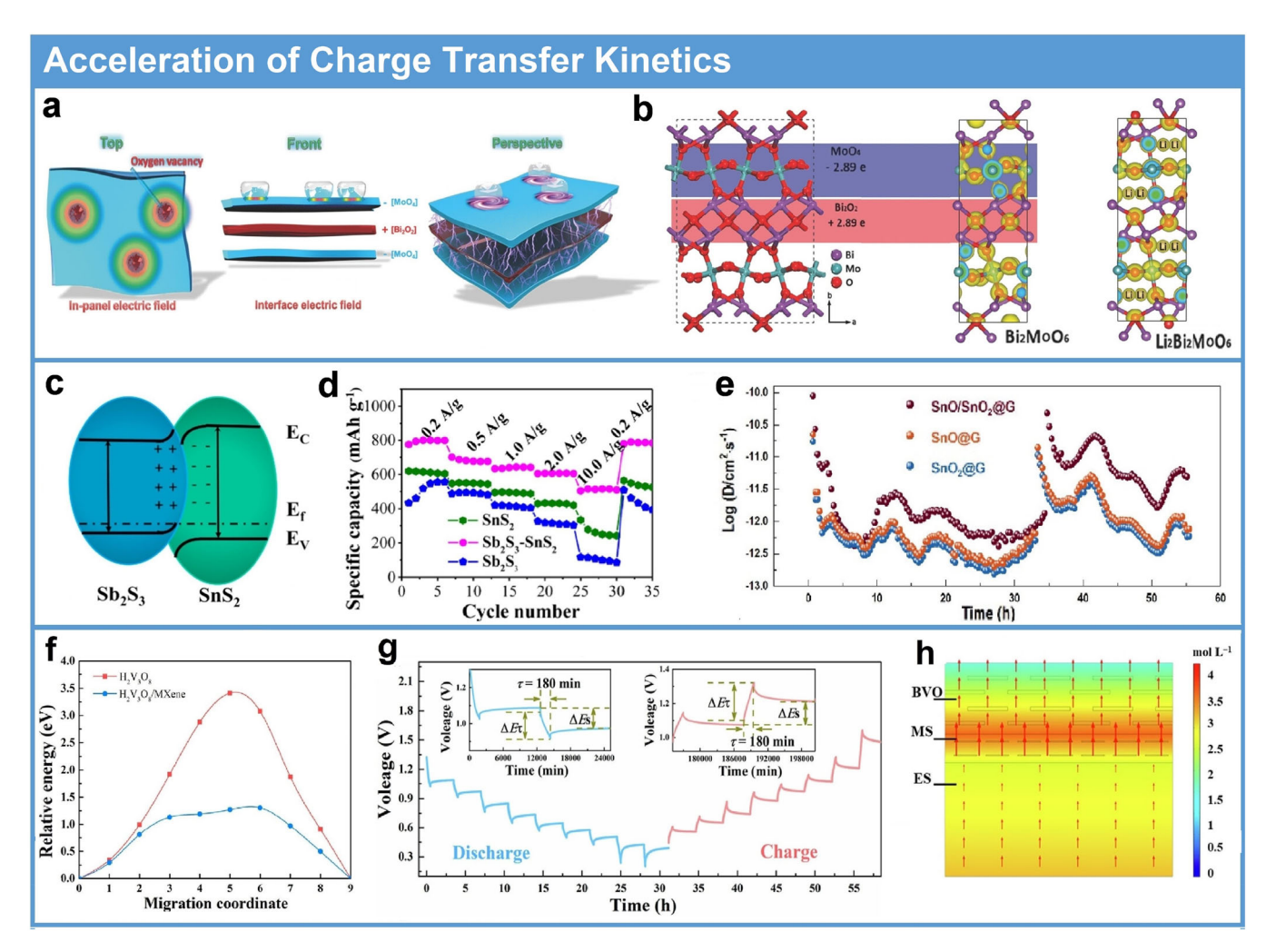


FIGURE 3 | (a) Schematic of the Structure and performance enhancement mechanism of the Bi_2MoO_6 . (b) Charge density distribution of Bi_2MoO_6 in the initial and the charged states [38]. Reproduced with permission: Copyright 2016, WILEY-VCH. (c) The direction of internal electric field, and (d) rate capability of the Sb_2S_3 - SnS_2 [39]. Reproduced with permission: Copyright 2019, Elsevier. (e) Li^+ diffusion coefficient in the $SnO/SnO_2@G$ [40]. Reproduced with permission: Copyright 2024, American Chemical Society. (f) The relative diffusion energy barrier at the $H_2V_3O_8/MX$ ene interface [42]. Reproduced with permission: Copyright 2022, Elsevier. (g) GITT profile, and (h) simulated electric field distribution in the BaV_6O_{16} - $3H_2O/MoS_2$ [44]. Reproduced with permission: Copyright 2025, Elsevier.

originates from geometric expansion of interstitial spaces and electron localization near OVs, collectively lowering migration barriers of K⁺ (Figure 4c). In another study, Zhang et al. [46] engineered MnO/MnS heterostructures encapsulated in pyrolytic carbon microspheres, where the interfacial synergy between sulfides and oxides reduces Li⁺ adsorption energy while accelerating diffusion kinetics (Figure 4d,e). The electrode demonstrates exceptional cyclability, delivering a stable discharge capacity of 522 mAh g⁻¹ at 3.0 A g⁻¹ over 2000 cycles with 85.6% capacity retention. The superior cycle performance originates from the unique electronic coupling at the interfaces, which stabilizes the electrode architecture during electrochemical cycling.

Recently, Li et al. [47] prepared a hierarchical architecture by epitaxially growing MoS_2 nanosheets on vanadium nitride (VN)-modified carbon cloth (CC) (Figure 4f). This bilayer configuration leverages synergistic interfacial coupling between VN and MoS_2 to establish shortcuts for rapid electron transfer and ion diffusion, achieving a discharge capacity of 258 mA h g⁻¹ at 50 mA g⁻¹. Chen et al. [48] demonstrated an organic-inorganic hybrid strategy

through core-shell MnO₂@PANI structures, where the polyaniline coating facilitated hydrated Zn²⁺ desolvation by coordinating water molecules while structurally stabilizing the MnO₂ core. Both DFT and experimental results confirmed enhanced Zn2+ diffusion kinetics and exceptional structural stability in the configuration, enabling 77% capacity retention after 1000 cycles (Figure 4g,h). Moreover, Jiang et al. [49] achieved covalent-bond-mediated interfacial stabilization in TiO2-based composites. Their approach involved spontaneous redox reactions between defect-rich active TiO2 and GO substrates, resulting in the formation of robust covalent linkages. These chemical bonds not only effectively stabilized the active species on the substrate but also enabled the exposure of abundant active sites during electrochemical cycling. Importantly, the established covalent interactions across the heterointerfaces were found to significantly facilitate ion transport throughout the composite structure.

Yang et al. [50] engineered a multiscale-tailored interface architecture in hierarchically porous VSe_{2-x}·nH₂O (Figure 5a), demonstrating exceptional all-climate Zn²⁺ storage capabilities.

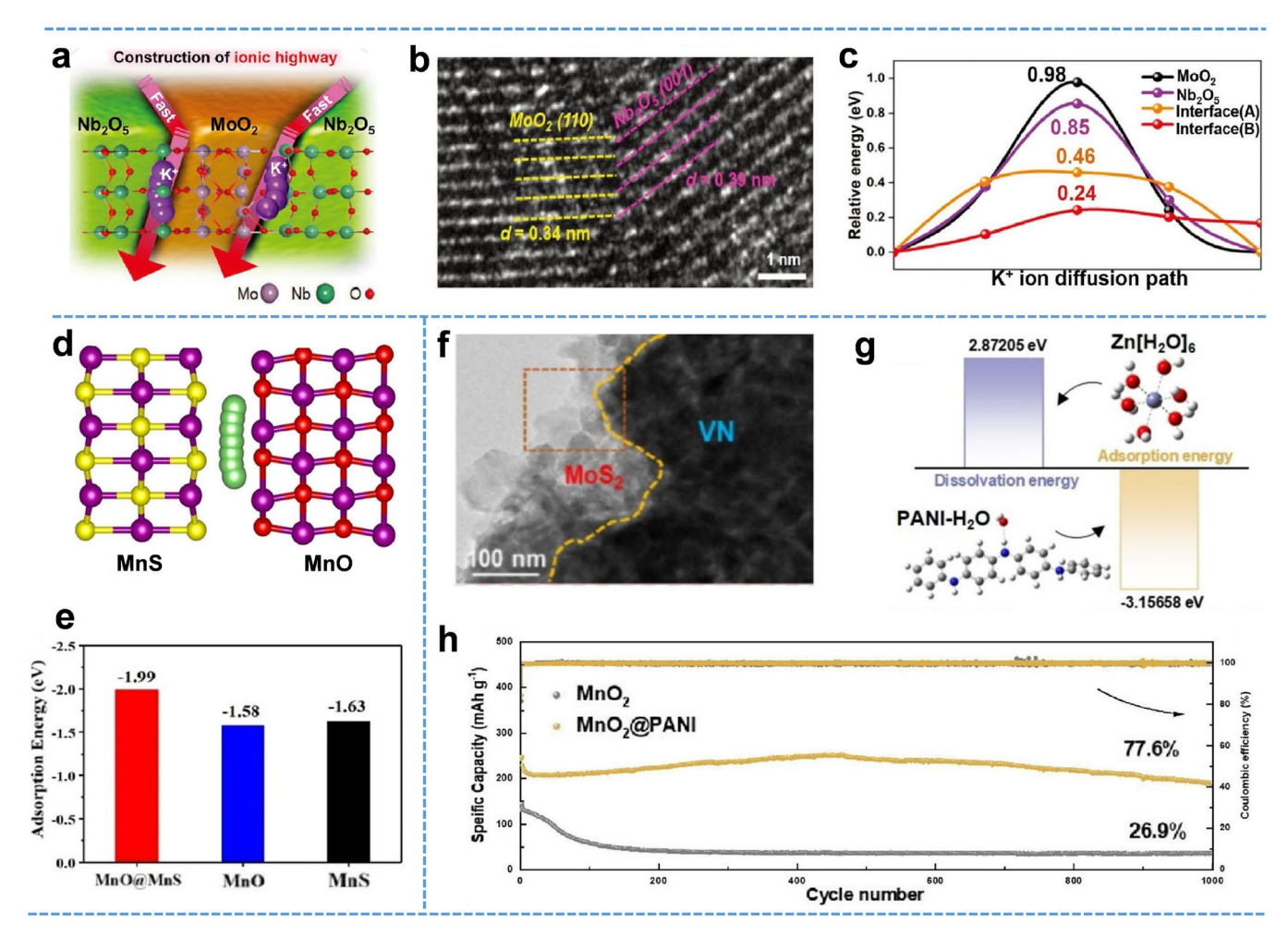


FIGURE 4 | (a) Schematic of K⁺ diffusion pathways in the Nb₂O₅/MoO₂, (b) HRTEM image of the Nb₂O₅/MoO₂ interface, and (c) theoretically calculated K⁺ migration barriers [45]. Reproduced with permission: Copyright 2022, WILEY-VCH. (d) Li⁺ migration pathways, and (e) Li⁺ adsorption energies in the MnO@MnS [46]. Reproduced with permission: Copyright 2022, American Chemical Society. (f) TEM image of the CC@ VN-MoS₂ [47]. Reproduced with permission: Copyright 2024, Elsevier. (g) Water adsorption energy of the PANI and water molecules. (h) Cycle performance at 2 A g^{-1} of the MnO₂@PANI electrode [48]. Reproduced with permission: Copyright 2025, Elsevier.

The synergistic interplay of Se vacancy-enriched atomic arrangement and intercalated H2O-induced shielding at the interface enhances Zn2+ adsorption capacity while reducing interlayer diffusion barriers (Figure 5b,c), thereby overcoming traditional kinetic limitations in layered chalcogenides. Li et al. [51] recently developed an α -MnO₂@ δ -MnO₂ homojunction material with varying crystallinities through an in-situ growth and annealing strategy. DFT calculations and structural analysis revealed that the interface, inherent to the MnO₂ homojunction, acts as an "electron pump", significantly facilitating electron transfer across the interface and enhancing ion transport kinetics (Figure 5d). Lv et al. [52] synthesized a MoS₂@EG composite by co-intercalating H₂O and ethylene glycol (EG) into the interlayers of MoS₂. As shown in Figure 5e, the composite exhibits significantly lower activation energy for interfacial Zn2+ transfer compared to pristine MoS₂, suggesting that solvated Zn²⁺ intercalated into MoS₂@EG, avoiding the energetically unfavorable desolvation process associated with high charge-transfer resistance. DFT calculations indicated that the EG and crystal H2O molecules mitigate the electrostatic interactions between the inserted Zn²⁺ and the electrode framework (Figure 5f), which accelerates Zn²⁺ diffusion and enhances the structural stability of the composite.

In summary, the rational engineering of heterointerfaces with tailored built-in electric fields and dimensionally optimized architectures has emerged as an effective approach to accelerate charge transfer kinetics. By decoupling the roles of electrons and ions in the interface region, heterostructures minimize cross-talk between ionic and electronic resistances, while localized electric fields synergistically lower migration barriers and amplify carrier flux. Recent advancements across multi-dimensional material systems demonstrate that interface engineering critically governs the storage kinetics, with the dimensional configuration of composite components exerting distinct yet profound influences on interfacial performance.

In homodimensional systems, where the constituents possess identical dimensionality, structural coherence through lattice matching minimizes interfacial defects. The resulting alignment of crystalline orientations facilitates uniform built-in electric fields, significantly enhancing ion diffusion kinetics. However, such systems inherently inherit the dimensional limitations of their components. For instance, 2D/2D or 1D/1D architectures exhibit geometrically constrained ion transport pathways, leading to kinetic bottlenecks under high-rate operation due to restricted

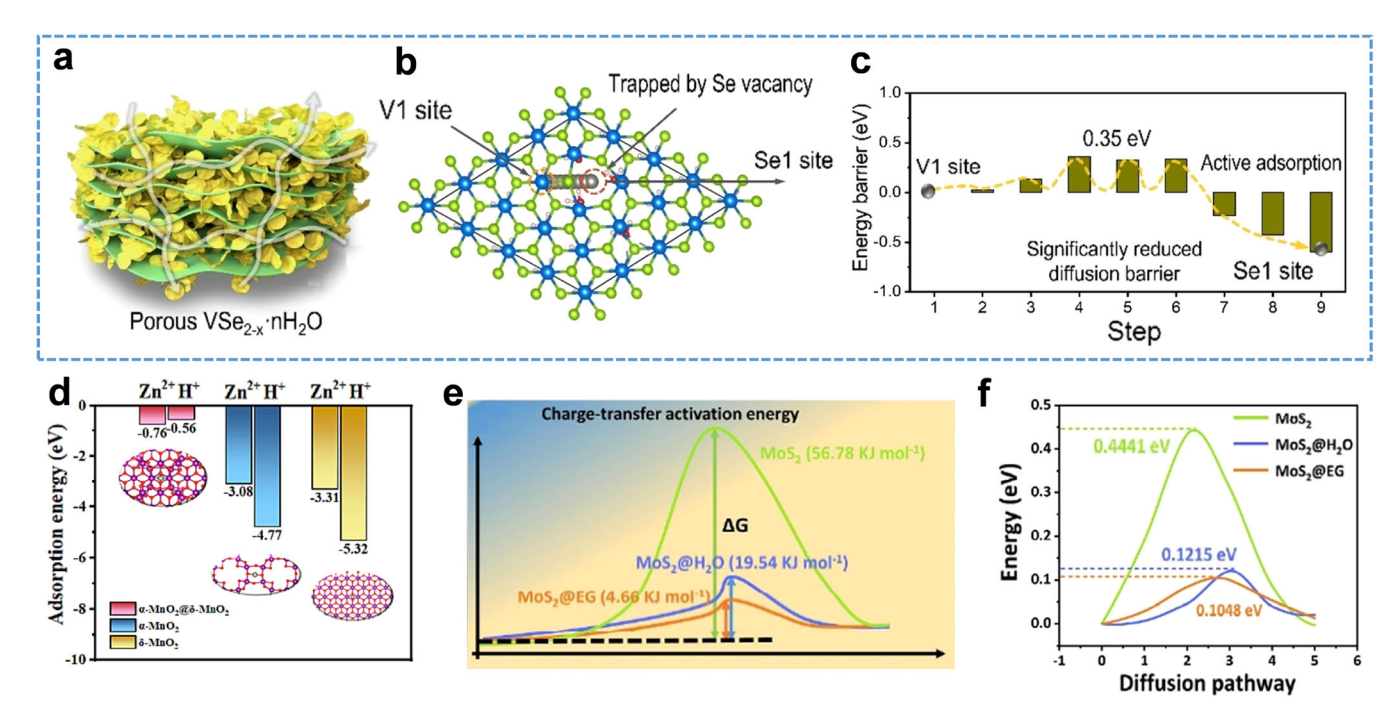


FIGURE 5 | (a) Schematic of the hierarchically porous $VSe_{2x} nH_2O$. (b, c) DFT calculations of Zn^{2+} diffusion pathways and corresponding energy barriers in the $VSe_{2x} nH_2O$ [50]. Reproduced with permission: Copyright 2023, WILEY-VCH. (d) DFT calculations of the adsorption energies of H^+ and Zn^{2+} of the α-MnO₂@δ-MnO₂ [51]. Reproduced with permission: Copyright 2024, Elsevier. (e) The calculated desolvation activation energies, and (f) diffusion barriers of Zn^{2+} in the MoS₂@EG [52]. Reproduced with permission: Copyright 2023, Springer.

spatial accessibility. In contrast, heterodimensional systems integrate components of differing dimensionalities, creating a hierarchical interplay between nanoscale quantum effects and macroscopic charge transport networks. Here, lower-dimensional units (e.g., 0D/1D) offer abundant active sites and surface-driven storage mechanisms, while higher-dimensional frameworks (e.g., 2D/3D) ensure continuous pathways for rapid carrier migration. This dimensional complementarity enables concurrent optimization of ion accessibility and electronic conductivity through multiscale porosity engineering. However, dimensional mismatch can introduce interfacial strain and defective boundaries, potentially undermining structural stability during extended cycling. Therefore, advanced interface modulation strategies are essential to reconcile the trade-off between multidimensional synergy and interfacial integrity.

These dimensional insights establish foundational principles for interface engineering, guiding the design of high-power battery systems. By elucidating structure-kinetics relationships, researchers can tailor interfacial configurations to simultaneously enhance charge transfer kinetics while maintaining an optimal balance between rate capability and long-term stability. Future efforts should focus on defect passivation techniques and strain-relief architectures to further harness the potential of hetero-dimensional systems.

3.2 | Expansion of Storage Capacity Beyond Bulk Limitations

Recent advancements in interfacial storage have challenged traditional thermodynamic limitations of energy storage materials by enabling charge storage through extended electrochemical zones that transcend bulk lattice constraints. Representative examples of interfacial storage that expand capacity are summarized in Table 2. To establish a systematic framework for understanding interfacial contributions to energy storage performance, it is necessary to distinguish between two distinct interfacial storage modes: interface-involved and interface-dominated storage. The former describes systems where interfacial effects supplement conventional bulk storage mechanisms, while the latter represents a paradigm shift where interfaces dominate the energy storage processes.

1. Interface-Involved Storage

In conventional composite systems, the limited interfacial density restricts the role of interfacial contributions, which typically serve as supplementary enhancements rather than the primary determinant of total storage capacity. Liang et al. [53] employed Nb-based cation-deficient perovskite oxides (Ce_{1/3}NbO₃) as an anode material capable of storing Na⁺ through intercalation reactions. The material contains a substantial number of cation vacancies in the Ce column (Figure 6a), which generate localized negative charge accumulation and induce the formation of space charge regions that attract and stabilize Na+ ions, thereby contributing to additional storage capacity (Figure 6b,c). Yang et al. [54] fabricated a mixed conductor comprising ultrathin SnO/C heterostructures on silicon surfaces. This electrode demonstrates a high Li+ storage capacity with ultralong cycle durability, achieved through synergistic bulk storage and interfacial job-sharing mechanisms at coupled heterointerfaces that critically enhance Li+ storage capability. Ma et al. [55] reported a 3D FeP/CoP heterostructure embedded within N-doped carbon aerogel. The

TABLE 2 | Interface engineering strategies to expand storage capacity.

| Material | Battery Type | SC/R | RT/CN/R | References |
|--|---------------|-----------|---------------|------------|
| Interface-Involved Storage | ; | | | |
| $Ce_{1/3}NbO_3$ | SIBs | 141/0.015 | 97%/10000/1.5 | [53] |
| SnO/C@Si | LIBs | 1251/0.1 | 100%/1000/1 | [54] |
| FeP/CoP | SIBs | 425/0.2 | 92%/8500/5 | [55] |
| Fe ₃ O ₄ /FeP@C | LIBs | 1081/0.1 | 100%/1000/2 | [56] |
| QFe ₃ O ₄ /SCNT/f-PANI | LIBs | 907/0.1 | 100%/1000/1 | [57] |
| P-TiO ₂ | SIBs | 400/0.05 | 79%/400/0.2 | [58] |
| MnO ₂ /GDY | LIBs | 660/0.2 | 100%/200/1 | [59] |
| Ni@TiO ₂ | LIBs | 391/0.2 | 55%/300/1 | [60] |
| ZnO-CuO | LIBs | 612/0.2 | 100%/900/0.5 | [61] |
| FeVO₄•nH₂O | SIBs and LIBs | \ | \ | [62] |
| MF-FC | LIBs | 1376/0.1 | 100%/300/2 | [63] |
| Interface-Dominated Stora | ige | | | |
| VO_x/rGO | AZIBs | 443/0.1 | \ | [64] |
| VO_x/GO | AZIBs | 464/0.1 | 86%/4000/10 | [35] |
| Fe/Li ₂ O | LIBs | 407/1 | 100%/30000/10 | [65] |
| PBA/rGO | SIBs | 128/0.034 | 81%/1000/1.7 | [19] |
| TOC-AI | AZIBs | 100/0.1 | 77%/17000/1 | [66] |

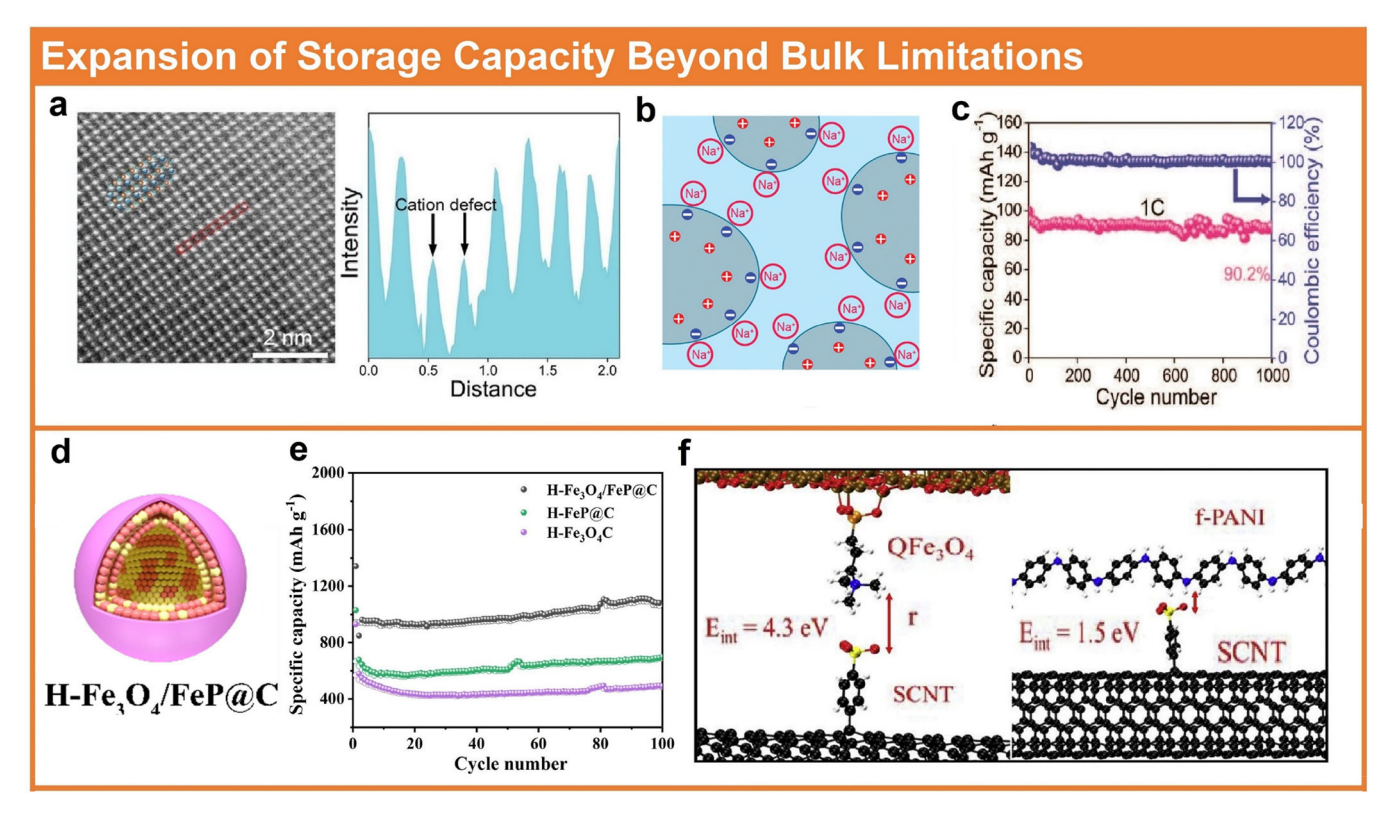


FIGURE 6 | (a) HAADF-STEM image and line profile acquired from the dashed region of the $Ce_{1/3}NbO_3$. (b) Schematic of space charge regions of the $Ce_{1/3}NbO_3$. (c) Cycle performance at 1 C of the $Ce_{1/3}NbO_3$ anode [53]. Reproduced with permission: Copyright 2022, WILEY-VCH. (d) Schematic of the $Fe_3O_4/FeP@C$ spheres, and (e) cycle performance at 0.1 A g^{-1} of the $Fe_3O_4/FeP@C$ electrode [56]. Reproduced with permission: Copyright 2022, Elsevier. (f) The interfacial intercalation energies of the QFe $_3O_4/SCNT/f$ -PANI [57]. Reproduced with permission: Copyright 2020, Elsevier.

well-designed atomic interface between FeP and CoP not only improves capacitive contributions through enhanced electron transport but also offers additional sites for Na⁺ adsorption. Recently, Yan et al. [56] prepared Fe₃O₄/ FeP@C spheres with heterogeneous hollow architectures (Figure 6d). Combined experimental characterizations and DFT calculations demonstrate that the heterointerface facilitates charge transfer while increasing active site availability, thus enhancing electrode capacity (Figures 6e). Liu et al. [57] developed a Fe₃O₄-based multiphase nanohybrid material (QFe₃O₄/SCNT/f-PANI) featuring ionically bonded interfaces, showcasing excellent cycling stability. The superior performance originates from significant pseudocapacitive contributions at the engineered interfaces with intrinsic self-healing properties, with supporting DFT simulations confirming the interfacial Li+ storage mechanism (Figure 6f).

In addition, Zhao et al. [58] reported nonporous bulk heterogeneous particles composed of a TiO2 matrix and phosphorus (P-TiO₂) with a 3D interface (Figure 7a). This interface acts as a rapid ion transport network and activates pseudocapacitive Na⁺ storage within the bulk, delivering a volumetric capacity exceeding 50% compared to commercial hard carbon (Figure 7b). The observed pseudocapacitive contribution originates from the composite interface. distinct from conventional nanostructured electrodes that rely on external surface redox reactions. Lin et al. [59] developed MnO₂ nanowire/graphdiyne composites (MnO₂/ GDY) via a solvothermal method (Figure 7c), demonstrating high capacities and exceptional rate capability. These improvements are attributed to synergistic effects between nanosized MnO2 and porous GDY. DFT calculations further elucidate the energy storage mechanism of the composite, revealing a job-sharing mode that offers additional

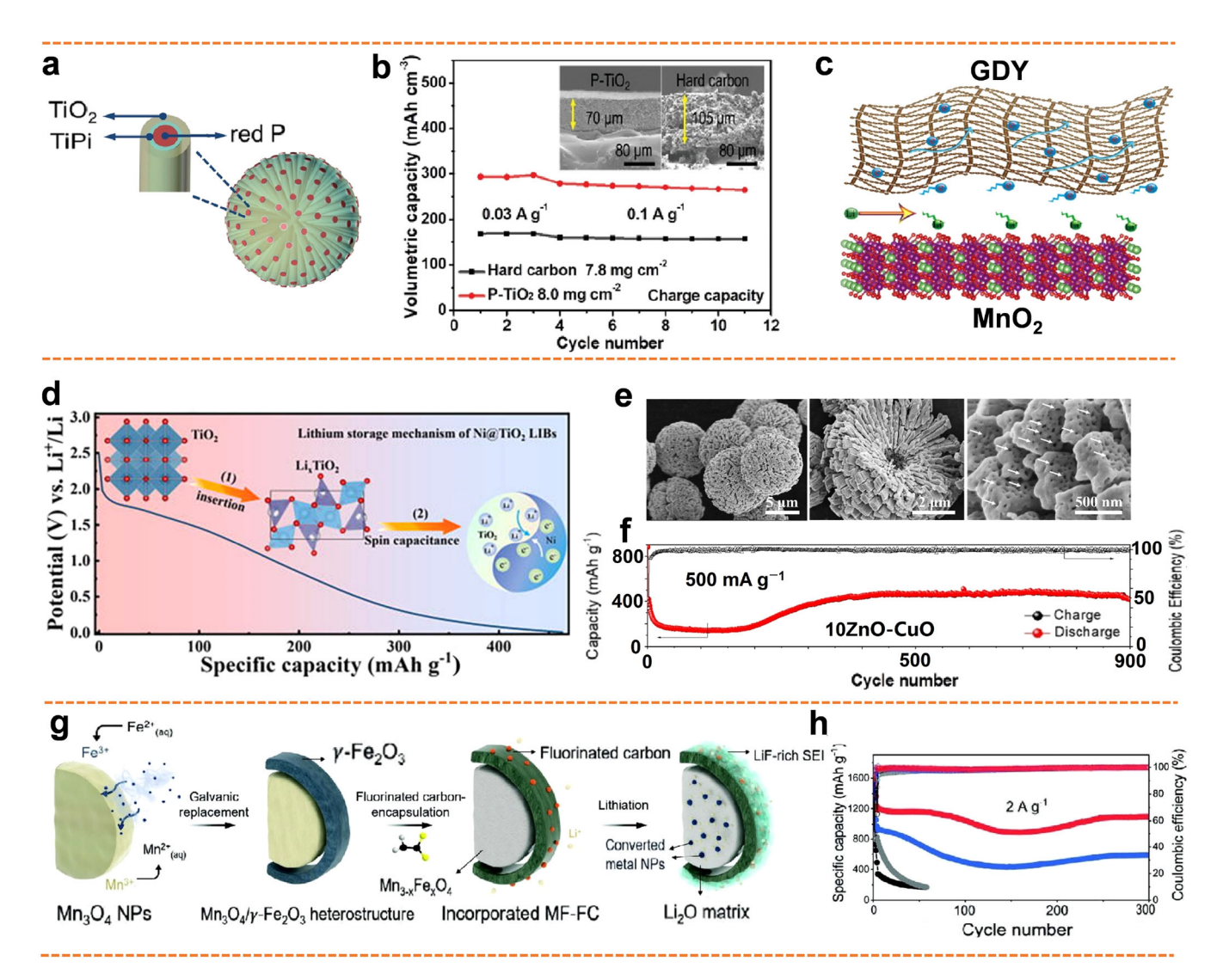


FIGURE 7 | (a) Schematic of the P-TiO₂ composite, and (b) volumetric capacities of the P-TiO₂ and hard carbon [58]. Reproduced with permission: Copyright 2020, WILEY-VCH. (c) Schematic of the MnO₂/GDY interfaces [59]. Reproduced with permission: Copyright 2020, Elsevier. (d) Schematic of lithium reaction mechanisms in the Ni@TiO₂ [60]. Reproduced with permission: Copyright 2024, AIP Publishing. (e) SEM images, and (f) cycle performance at 5 A g^{-1} of the ZnO-CuO [61]. Reproduced with permission: Copyright 2019, Elsevier. (g) Schematic of the synthesis process, and (h) cycle performance at 2 A g^{-1} of the MF-FC [63]. Reproduced with permission: Copyright 2024, WILEY-VCH.

Li⁺ storage. Chen et al. [60] engineered a Ni@TiO₂ anode with a yolk-shell structure. The composite, leveraging a synergistic storage mode with Ni as the electron-accepting phase and TiO₂ as the Li⁺-accepting phase, utilizes space charge storage from dual-phase conduction to provide additional capacity (Figure 7d).

Recently, Zhang et al. [61] reported a bottom-up synthesis strategy to fabricate a ZnO-CuO composite with a hierarchical architecture, comprising radially oriented macroporous spheres with central cavities (Figure 7e). The intergrowth of components generates abundant nanoscale heterointerfaces, which contribute to extra Li⁺ storage capacity (Figure 7f). Zhao et al. [62] performed DFT calculations and thermodynamic fitting on FeVO₄·nH₂O nanowires, validating a Li⁺ storage mechanism based on job-sharing dynamics. These theoretical investigations confirmed dual-phase interface formation during Li⁺ storage and revealed deeper conversion processes during lithiation compared to sodiation. To amplify interfacial effects for superior Li+ storage, Kang et al. [63] synthesized fluorinated carbon-modified manganese ferrites (MF-FC) through an electrochemical displacement reaction combined with fluorinated carbon encapsulation (Figures 7g). The spin-polarized surface capacitive effect induced by manganese ferrites, coupled with highly polarized interfacial sites from electronegative fluorinated carbon layer, significantly enhances space charge storage. This mechanism enables Li+ storage capacity exceeding theoretical predictions (Figures 7h).

2. Interface-Dominated Storage

In contrast to conventional composites constrained by limited interfacial density, the rational design of composites with interfacial architectures comparable in scale to their bulk constituents enables a fundamental transition in energy storage mechanisms from bulk-governed processes to interface-dominated behavior. This transition underscores the critical need for developing advanced composite systems with precisely engineered interfacial configurations. Through the construction of hierarchical architectures that synergistically integrate optimized interfacial networks and tailored electronic states, researchers can fully exploit interfacial storage potential, thereby overcoming the intrinsic energy storage limitations inherent to bulk-material systems.

Dai et al. [64] pioneered a VO_x sub-nanometer cluster/rGO composite for AZIB cathode (Figure 8a). In this architecture, the VO_x sub-nanometer clusters were tightly anchored onto rGO nanosheets through V-O-C bonds, forming atomic composite interfaces with sizes comparable to those of VO_x bulk. They demonstrated that Zn²⁺ is predominantly stored at the interface between VOx and rGO, which allows for decoupled transport of electrons and Zn²⁺ in the interfacial space charge regions, resulting in Zn²⁺ diffusion coefficients in the interface that are two orders of magnitude higher than those in the bulk. This interface-dominated storage mechanism achieves a remarkable electrochemical performance than conventional bulk mechanisms, including a high capacity of 443 mAh g⁻¹ at 100 mA g⁻¹ and outstanding rate capability of $174 \,\mathrm{mAh}\,\mathrm{g}^{-1}$ at $100 \,\mathrm{A}\,\mathrm{g}^{-1}$ (Figure 8b). Subsequent research extended this paradigm to a VO_y/GO composite with hydrogen-bonding interfaces [35]. These interfaces, characterized by their reversibility, universality, self-healing nature, and high per-volume concentration, represent an ideal model for interfacial storage research. In addition, these authors have introduced micropores on the surface of GO to expedite the penetration of Zn²⁺ through the carbon ring plane of GO (Figure 8c.d). This allows Zn²⁺ to be rapidly inserted in the interface between VO_x and GO in a given charging/discharging duration, thereby avoiding the capacity loss that typically occurs in bulk materials due to

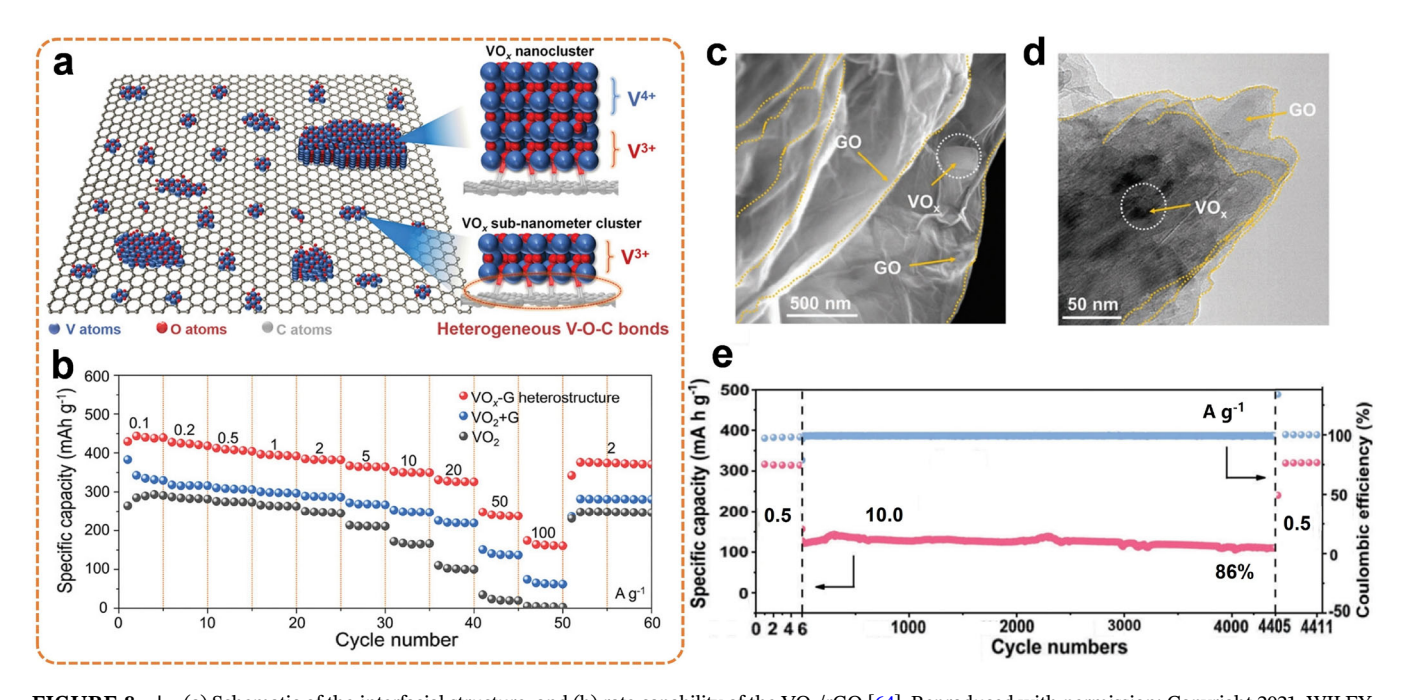


FIGURE 8 (a) Schematic of the interfacial structure, and (b) rate capability of the VO_x/rGO [64]. Reproduced with permission: Copyright 2021, WILEY-VCH. (c) SEM image, (d) TEM image, and (e) cycle performance at 10 A g⁻¹ of the VO_x/rGO [35]. Reproduced with permission: Copyright 2024, WILEY-VCH.

insufficient delivery of ions. The engineering feats facilitate ultrafast $\mathrm{Zn^{2+}}$ storage in the interfaces, outperforming bulk mechanisms through spatially decoupled transport and storage pathways for $\mathrm{Zn^{2+}}$ and electrons (Figure 8e). DFT calculations revealed that an optimal hydrogen-bond number is critical to maintaining interfacial reversibility, while carbon vacancies localized near the interfacial bonds in the GO plane were found to enhance interfacial storage capacity by modulating charge distribution.

Very recently, Zhao et al. [65] designed a Fe/Li₂O mixed conductor with optimized interfacial configuration, leveraging thermodynamic analyses to validate its interface-dominated storage mechanism. The spatial distribution of components creates a pronounced confinement effect that effectively maintains functional interfaces throughout cycling (Figure 9a–c), which is critical for achieving exceptional rate capability and long-term stability. Remarkably, the electrode demonstrates a reversible capacity of $126 \, \text{mAh} \, \text{g}^{-1}$ with an ultrafast charge/discharge time of just 6 s at $50 \, \text{A} \, \text{g}^{-1}$ (Figure 9d). Similarly,

Zhang et al. [19] utilized Prussian blue analogues (PBAs) and rGO to construct an artificial mixed conductor. The charge redistribution between PBAs and rGO in the composite interface allows for the decoupling of ion and electron pathways in the interfacial space charge regions. This composite electrode delivers a high capacity of 128 mAh g⁻¹ over 100 cycles, exhibiting remarkable stability with only 3% capacity loss. Notably, the interfacedominated storage mechanism has been successfully extended to traditionally inactive materials, dramatically expanding its applicability in EES systems. A breakthrough example is the TiO2-based cathode (TOC-AI) for AZIBs [66]. In the optimized composite architecture (Figure 9e-g), ultrafine TiO₂ nanocrystals (< 10 nm) are uniformly embedded within an amorphous carbon matrix, creating a continuous conductive network and abundant heterointerfaces. This atomic interface contact and strong interactions between the TiO2 nanocrystals and the carbon matrix establish efficient Zn2+ transport pathways, yielding a high capacity of 111 mAh g⁻¹ at 0.1 A g⁻¹ (Figure 9h) and excellent rate capability. Thermodynamic

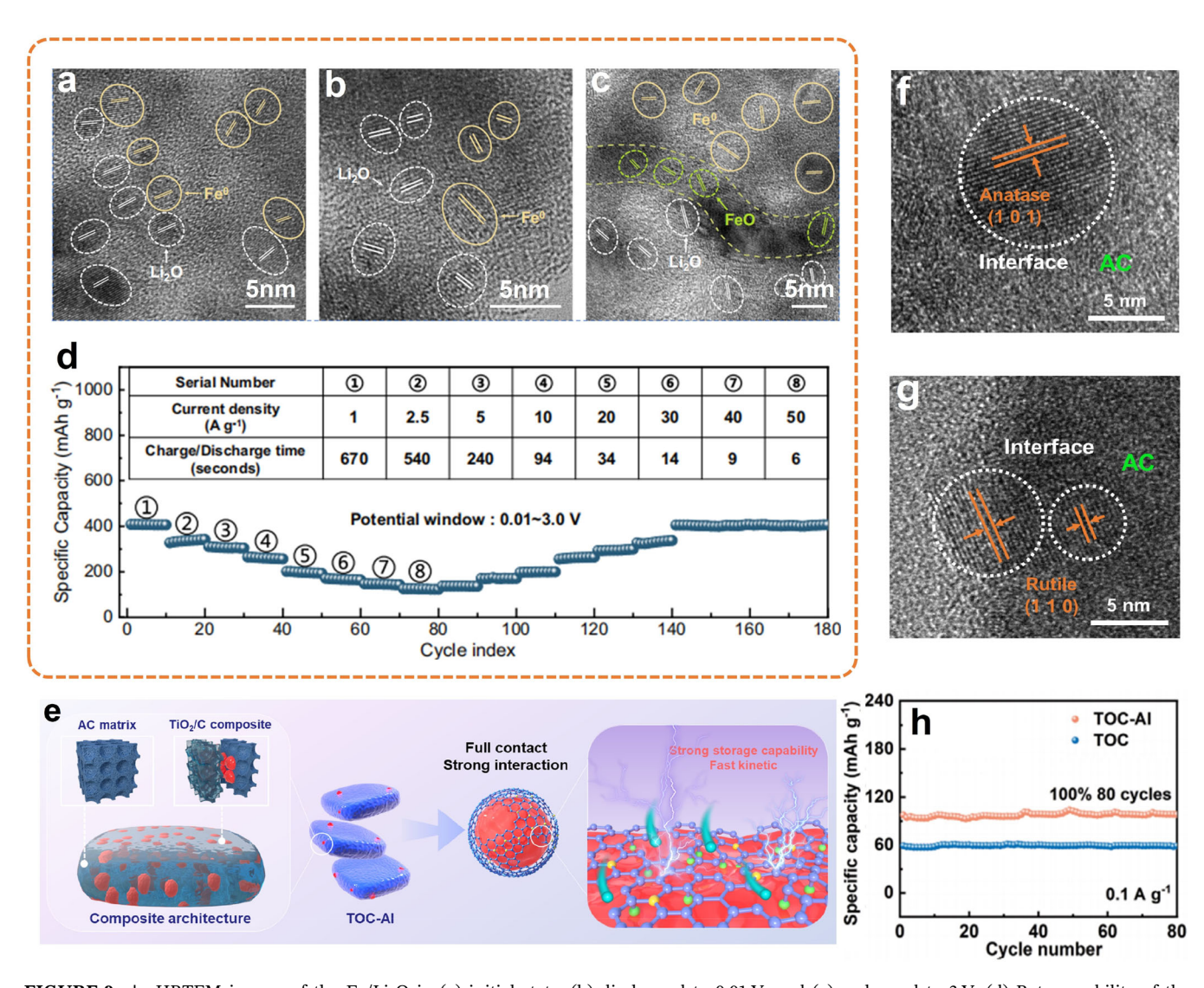


FIGURE 9 | HRTEM images of the Fe/Li₂O in (a) initial state, (b) discharged to 0.01 V, and (c) recharged to 3 V. (d) Rate capability of the Fe/Li₂O [65]. Reproduced with permission: Copyright 2024, Springer. (e) Schematic structures, (f, g) HRTEM images, and (h) cycle performance at $0.1 \, \text{Ag}^{-1}$ of the TOC-AI [66]. Reproduced with permission: Copyright 2024, WILEY-VCH.

fitting confirmed that Zn²⁺ storage primarily occurs at the heterointerface, aligning with the job-sharing mechanism.

The expansion of energy storage capacity through interfacial mechanisms presents a transformative approach to overcoming the inherent limitations of bulk material systems. By distinguishing between interface-involved and interfacedominated storage modes, a systematic framework emerges to guide the rational design of advanced energy storage materials. The distinction between the two interfacial storage modes lies in the relative contribution of interfacial mechanisms to the overall energy storage process. Interface-involved storage operates as a supplementary mechanism, where interfacial effects enhance bulk storage by introducing additional charge accommodation sites or improving charge transfer kinetics. This mode is typically observed in conventional composite systems with limited interfacial density, where bulk processes remain the primary storage pathway. In contrast, interfacedominated storage represents a transformative approach where energy storage is governed by engineered interfacial architectures rather than bulk properties. Here, interfaces are intentionally scaled and optimized to surpass bulk limitations, enabling spatially decoupled ion/electron transport pathways, enhanced capacitive contributions, and confinement effects that stabilize storage kinetics.

The application of these modes depends on the desired performance objectives. Interface-involved storage is suited for incremental improvements in systems where bulk mechanisms already provide a functional baseline. Interface-dominated storage, however, is critical for achieving breakthroughs in high-rate capability or long-term cyclability, particularly in systems constrained by slow bulk diffusion or irreversible phase transitions. By deliberately tailoring interfacial configurations, such as atomic-scale interfaces, space charge regions, or hierarchical conductive networks, researchers can shift the storage paradigm from bulk-dependent to interface-driven processes, unlocking new possibilities beyond conventional thermodynamic limits.

3.3 | Reinforcement of Structural Stability

The structural integrity of composite electrodes during cycling is governed by the mechanical and chemical stability of hetero-interfaces, which regulate stress distribution, interfacial reaction kinetics, and defect evolution [67]. Heterointerfaces act as dynamic

buffering zones, alleviating localized mechanical stresses generated by repetitive volume changes while suppressing deleterious side reactions through tailored chemical passivation. Engineered interfaces with optimized adhesion energy and elastic moduli can mitigate crack initiation and propagation by redistributing strain across electrode architectures, thereby preventing particle detachment or electrolyte penetration [68, 69]. Meanwhile, chemically stable interfaces may inhibit parasitic reactions by reducing uncontrolled electron and ion migration, preserving bulk electroactive phases [70]. Advanced interfacial designs, such as gradient compositional transitions [34] or self-healing chemistries [71, 72], can further enhance durability. These multifunctional roles collectively stabilize electrode structures against degradation, enabling extended cycle life and capacity retention. Representative interface engineering strategies for structural stabilization are summarized in Table 3.

Li et al. [73] designed multi-interfacial FeSe₂/CoSe₂ nanoparticles anchored on V₄C₃T_x nanosheets (Figure 10a), where interfacial Fe-Co bonds mitigate lattice strain during Na+ insertion/extraction while suppressing particle detachment, thereby achieving a high specific capacity of 450 mAh g⁻¹ after 1000 cycles at 1 A g⁻¹ and 260.5 mAh g⁻¹ after 15,000 cycles at 10 A g⁻¹(Figure 10b). Liu et al. [74] developed Ti₃C₂T_x-coated V₂O₅ nanoplates via van der Waals self-assembly, with the interface acting as both a physical barrier against vanadium dissolution and a chemical trap for vanadyl ions. demonstrating 99.5% capacity retention after 5000 cycles. Yuan et al. [75] fabricated VO₂ nanobelts uniformly coated with a single-atom cobalt-decorated N-doped carbon (VO₂@Co-N-C). Experimental results and DFT simulations (Figure 10c,d) revealed that the interfacial Co-O-V bonds play a critical role in mitigating structural distortion, effectively preventing VO₂ collapse and enhancing Zn²⁺ diffusion kinetics, which enables remarkable cycling stability, sustaining performance over 8,000 cycles at 20 A g⁻¹. Fang et al. [76] recently constructed a covalent heterostructure cathode for AZIBs that achieves unprecedented cycling stability. The innovation centers on the chemical growth of VO2 nanoarrays on MXene nanosheets (Figure 10e), inducing interfacial Ti-O-V asymmetric orbital hybridization, which significantly stabilizes OVs in the VO2 lattice. Leveraging this advanced architecture, the resulting MXene-VO_{2-x} exhibit exceptional reversibility and retain 98.6% of their initial capacity over 30,000 cycles at 20 A g⁻¹ (Figure 10f), accompanied by negligible structural degradation.

In some composite electrodes, dynamic breakage/reconstruction of interfacial bonds—termed "interface breathing"—can effectively accommodate volumetric strain during cycling while

TABLE 3 | Interface engineering strategies to reinforce structural stability.

| Material | Battery Type | SC/R | RT/CN/R | References |
|--|--------------|---------|--------------|------------|
| FeSe ₂ /CoSe ₂ @V ₄ C ₃ T _x | SIBs | 472/0.1 | 72%/15000/10 | [73] |
| $Ti_3C_2T_x/V_2O_5$ | AZIBs | 345/0.1 | 100%/5000/10 | [74] |
| VO ₂ @Co-N-C | AZIBs | 422/1 | 100%/200/1 | [75] |
| MXene-VO _{2-x} | AZIBs | 487/0.2 | 99%/30000/20 | [76] |
| VO_x/rGO | AZIBs | 443/0.1 | \ | [64] |
| VO _x /GO | AZIBs | 464/0.1 | 86%/4000/10 | [35] |
| V_5O_{12} ·6 H_2O @ Ti_3C_2 | AZIBs | 450/0.2 | 89%/1000/5 | [77] |

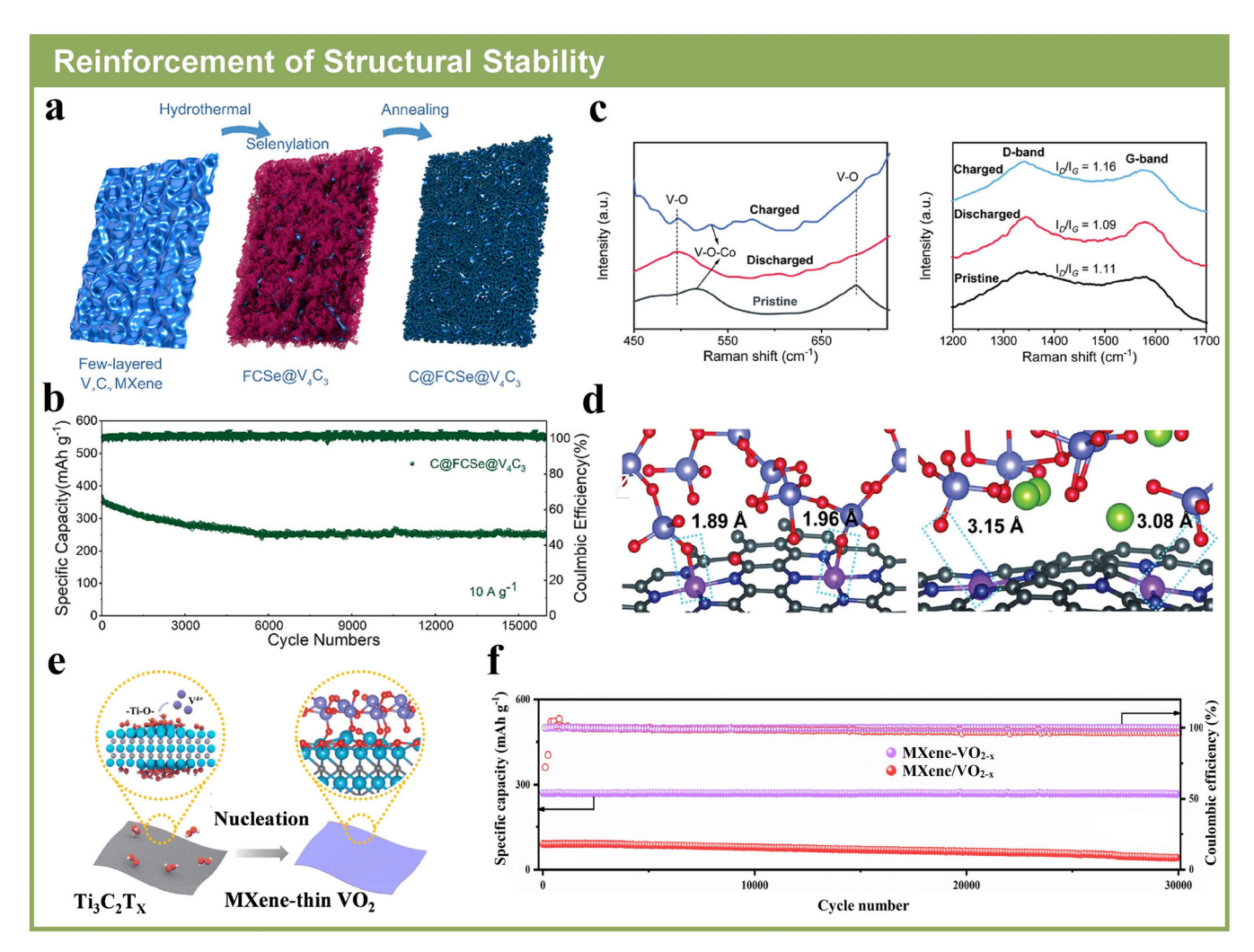


FIGURE 10 | (a) Schematic of the synthesis process, and (b) cycle performance at $10 \, \mathrm{Ag^{-1}}$ of the FeSe₂/CoSe₂@V₄C₃T_x [73]. Reproduced with permission: Copyright 2024, American Chemical Society. (c) Ex situ Raman spectra, and (d) DFT simulations of the VO₂@Co-N-C in the pristine and discharged/charged states [75]. Reproduced with permission: Copyright 2024, WILEY-VCH. (e) Schematic of VO₂ nanoarrays on MXene nanosheets, and (f) cycle performance at $20 \, \mathrm{Ag^{-1}}$ of the MXene-VO_{2-x} [76]. Reproduced with permission: Copyright 2022, The Royal Society of Chemistry.

generating supplementary ion storage sites. For example, in the VO_x/rGO composite [64], discharging induces cleavage of V-O-C bonds at the heterointerface (Figure 11a-d), accompanied by increased V-O-Zn bonding. Upon Zn²⁺ extraction, V-O-C bonds reconstruct, demonstrating reversible interfacial adaptability. Our recent investigation highlights that pure VO_x electrode suffers from vanadium dissolution and irreversible structural degradation [35], while the VO_x/GO composite utilizes reversible breakage/ reconstruction of interfacial hydrogen bonds during Zn2+ storage (Figure 11e,f), significantly improving structural stability. Xiao et al. [77] also observed analogous interface breathing phenomenon in the V₅O₁₂·6H₂O@Ti₃C₂ composite, where dynamic breakage/reconstruction of interfacial V-O-Ti bonds during Zn²⁺ insertion/extraction reduces structural stress, achieving 88.9% capacity retention after 1000 cycles at 5 A g⁻¹ (Figure 11g). Further validity of interface breathing was observed in the VO₂/Co-N-C interface [75], where Zn²⁺ insertion triggers progressive, reversible breaking of the Co-O-V bonds (Figure 11h), showing the interfacial flexibility to balance ion storage and mechanical resilience.

The structural stability of composite electrodes during electrochemical cycling is critically dependent on the rational engineering of heterointerfaces, which serve dual mechanical and chemical roles. Mechanically, interfaces act as dynamic stress buffers, redistributing strain to mitigate crack formation and particle detachment caused by repetitive volume changes. Chemically, stable interfaces suppress parasitic reactions by regulating ion/electron migration and passivating reactive surfaces. A notable recent innovation is interface breathing, where reversible bond breakage and reconstruction at heterointerfaces dynamically accommodate volumetric strain while generating extra ion storage sites. These interfacial mechanisms stabilize electrode architectures, enabling extended cycle life by balancing electrochemical activity with structural resilience. The integration of such multifunctional interfaces underscores their pivotal role in advancing robust, long-lasting energy storage systems.

3.4 | Suppression of Space Charge Effects at Electrolyte/Electrode Interfaces

A critical distinction between solid-state and conventional liquid-electrolyte batteries lies in their interfacial challenges.

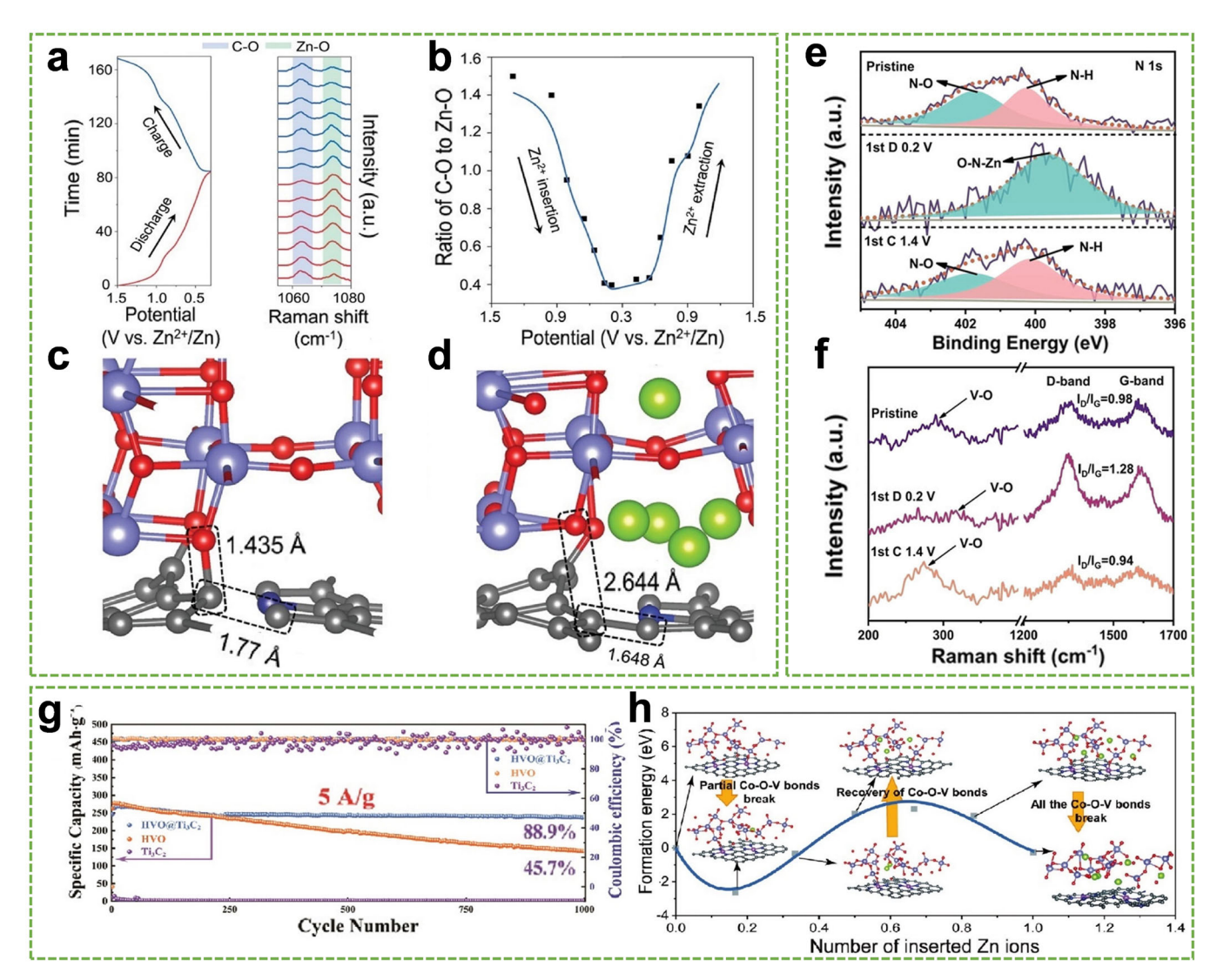


FIGURE 11 (a) In Situ Raman spectra, (b) quantitative ratio of the C-O to Zn-O bonds during discharge/charge, and (c, d) DFT simulations of the interfacial bonding configurations in the pristine and discharged states of the VO_x/rGO [64]. Reproduced with permission: Copyright 2021, WILEY-VCH. (e) Ex Situ XPS spectra of N 1s and (f) Ex Situ Raman spectra of the VO_x/rGO [35]. Reproduced with permission: Copyright 2024, WILEY-VCH. (g) Cycle performance at 5 A g^{-1} of the $V_5O_{12} \cdot 6H_2O@Ti_3C_2$ [77]. Reproduced with permission: Copyright 2023, WILEY-VCH. (h) Formation energy evolution upon Zn^{2+} intercalation in the $VO_2@Co-N-C$ interface [75]. Reproduced with permission: Copyright 2023, WILEY-VCH.

In solid-state systems, the inherent rigidity of both solid electrolytes and electrodes prevents the formation of intimate atomic-level contact achievable in liquid-based systems. Unlike liquid electrolytes that conform to surface irregularities through fluidity, solid electrolytes lack self-healing interfacial adaptability, leading to incomplete electrode-electrolyte contact and increased interfacial impedance. Furthermore, the formation of space charge regions at electrolyte/electrode interfaces introduces an additional energy barrier for charge transfer. These interfacial electric fields arise from electrochemical potential mismatches between components, forcing ions to overcome built-in potential gradients during interphase transport, contrasting with the rapid charge transport observed at internal electrode interfaces, where space charge regions enhance ionic conductivity. Recent advances in solid-state electrolyte engineering have unveiled promising strategies to address these interfacial issues. This section critically examines emerging approaches to suppress deleterious space charge effects in recent literature, focusing on interfacial modification

techniques of ceramic-based electrolytes to reconcile ion transport kinetics with thermodynamic stability in solid-state batteries.

Shi et al. [78] developed a novel composite solid electrolyte (PVBL) by incorporating ${\rm BaTiO_3\text{-}Li_{0.33}La_{0.56}TiO_{3-x}}$ (BTO-LLTO) nanowires into a PVDF matrix (Figure 12a). They use the polarized BTO to enhance Li-salt dissociation, producing mobile ${\rm Li^+}$ that spontaneously migrate to the adjacent LLTO phase for rapid conduction. Simultaneously, the BTO-LLTO effectively suppresses the formation of space charge regions at the composite interface. The coupling effects endow PVBL with exceptional room-temperature ionic conductivity ($8.2 \times 10^{-4} \, {\rm S \, cm^{-1}}$) and ${\rm Li^+}$ transference number (0.57). Furthermore, the PVBL electrolyte demonstrates excellent interfacial stability by homogenizing the electric field distribution at electrode interfaces, thus enabling remarkable cycling performance with stable operation for 1,900 h at 0.1 mA cm⁻² in Li/PVBL/Li symmetric cells (Figure 12b). Shortly afterward, Ma et al. [79]

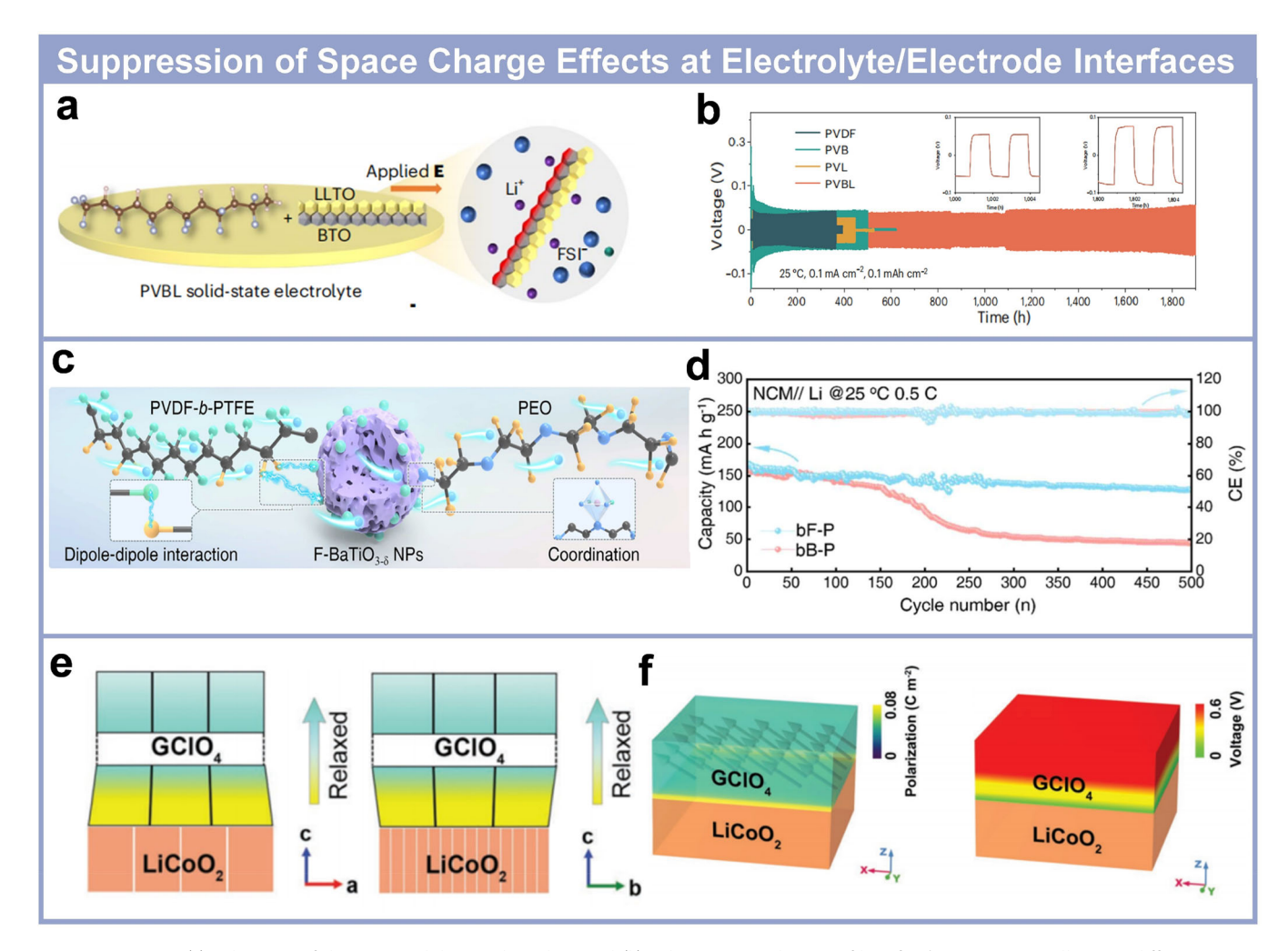


FIGURE 12 | (a) Schematic of the PVBL solid-state electrolyte, and (b) galvanostatic voltage profiles of Li/Li symmetric cells using different PVDF-based electrolytes at 0.1 and 0.1 mAh cm⁻² [78]. Reproduced with permission: Copyright 2023, Springer. (c) Schematic of the F-BTO, and (d) cycle performance at 0.5 C of the NCM//Li batteries [79]. Reproduced with permission: Copyright 2023, American Chemical Society. (e) Schematic of the cell distortion of GClO₄ coatings, and (f) the phase-field simulation of the GClO₄ and LiCoO₂ [81]. Reproduced with permission: Copyright 2023, WILEY-VCH.

designed a fluorinated dielectric electrolyte (F-BTO) by combining PVDF-b-PTFE with PEO to establish stable cross-phase Li $^+$ conduction pathways (Figure 12c), achieving an enhanced room-temperature ionic conductivity of $5.640 \times 10^{-4}\,\mathrm{S\,cm^{-1}}$. Additionally, this electrolyte system exhibits superior dynamic interface stability by suppressing cathode space charge regions and alleviating anode internal stress, leading to outstanding cycling performance (Figure 12d). Around the same time, Xiao et al. [80] demonstrated that incorporating dielectric BTO into a polymer-based composite solid-state electrolyte not only effectively suppressed the space charge effect at the cathode/electrolyte interface but also significantly enhanced high-voltage stability. Consequently, the BTO-modified solid-state battery exhibited exceptional cycling stability, achieving 1800 and 1300 cycles under high cut-off voltages of 4.6 and 4.7 V, respectively.

Recently, Li et al. [81] developed an innovative ferroelectric guanidinium perchlorate (GClO $_4$) coating to address interfacial instability between LiCoO $_2$ cathodes and Li $_6$ PS $_5$ Cl electrolytes. Their study reveals that the flexoelectric effect, induced by the lattice mismatch between GClO $_4$ and LiCoO $_2$, stabilizes the GClO $_4$ coating in a single-domain state with upward self-polarization (Figure 12e). This generates a vertically downward

built-in electric field relative to the cathode, effectively driving Li⁺ into the electrolyte toward the three-phase interface and mitigating the space charge effect (Figure 12f). As a result, the GClO₄-coated battery achieves a significantly enhanced initial discharge capacity of 210.6 mAh g⁻¹ at 0.1 C, far surpassing the 161.1 mAh g⁻¹ of the uncoated counterpart. Chen et al. [82] fabricated a LiNbO₃-coated NCM cathode, enabling intimate contact with the Li₆PS₅Cl electrolyte. By regulating the coating effects, the thickness of the space charge region can be controlled throughout the process, ensuring rapid Li⁺ migration across the interface. This optimization led to outstanding cycling stability, with 90.6% capacity retention after 100 cycles and a high retained capacity of 136.2 mAh g⁻¹ even after 800 cycles.

Similarly, Liu et al. [83] devised a sulfide surface coating for single-crystal Li[Ni $_{0.9}$ Co $_{0.05}$ Mn $_{0.05}$]O $_2$ (SC-NCM90) cathode to enhance interfacial stability with Li $_6$ PS $_5$ Cl solid electrolyte. The sulfide coating effectively suppresses detrimental interfacial reactions between Li $_6$ PS $_5$ Cl and the oxide cathode while significantly mitigating the space charge effect, thereby facilitating rapid Li $^+$ transport and inhibiting impedance growth during cycling. Further extending this strategy, the same group designed a hybrid Li $_3$ PO $_4$ and Li $_3$ BO $_3$ coating for ultrahigh-nickel single-crystal

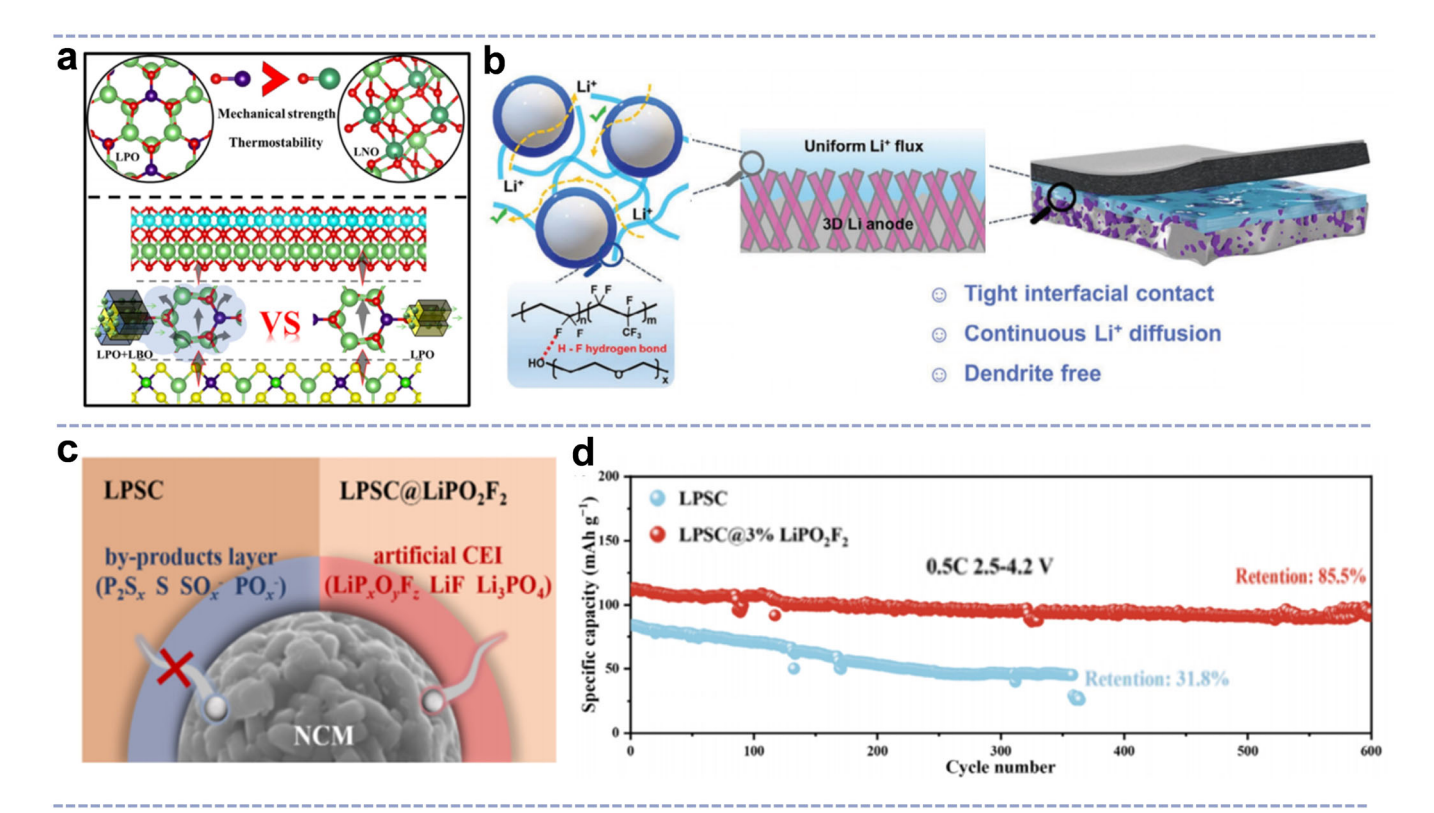


FIGURE 13 | (a) Advantages of hybrid Li₃PO₄ and Li₃BO₃ coatings [84]. Reproduced with permission: Copyright 2025, WILEY-VCH. (b) Schematic of the polymer coating LLZTO electrolyte [85]. Reproduced with permission: Copyright 2024, WILEY-VCH. (c) Design concept of cathode/electrolyte interface, and (d) cycle performance at 0.5 C of Li_{5.5}PS_{4.5}Cl_{1.5}@3%LiPO₂F₂ and Li_{5.5}PS_{4.5}Cl_{1.5} [86]. Reproduced with permission: Copyright 2025, WILEY-VCH.

LiNi $_{0.92}$ Co $_{0.06}$ Mn $_{0.02}$ O $_2$ (SC-NCM92) cathode [84]. This dual-coating system synergistically enhances interfacial ionic conductivity and mechanical strength while alleviating structural degradation and space charge effects (Figure 13a). Consequently, the hybrid-coated cathode achieves an exceptional discharge capacity of 225 mAh g $^{-1}$ at 0.1 C, along with significantly improved rate capability and long-term cycling stability.

Shen et al. [85] proposed an innovative strategy involving the construction of a polymer layer on the Li_{6.4}La₃Zr_{1.4}Ta_{0.6}O₁₂ (LLZTO) electrolyte (Figure 13b), which serves as a coherent interfacial region to suppress space charge region formation by mitigating electron localization. Through conjugate hybridization of fillers, this approach not only alleviates particle aggregation but also promotes Li-salt dissociation, thereby reducing interfacial resistance between the ceramic filler and polymer matrix. The resulting hybrid solid electrolyte demonstrates remarkable performance, achieving a high ionic conductivity of 0.47 mS cm⁻¹ and an ion migration number of 0.78 at room temperature. When integrated into a Li//Li symmetric cell, the electrolyte enables stable cycling with a high critical current density of 2.0 mA cm⁻². Moreover, NCM//Li batteries employing this electrolyte exhibit exceptional long-term stability, retaining capacity over 500 cycles at 0.5 C. In contrast to complex coating techniques, Wu et al. [86] introduced a LiPO₂F₂ additive strategy to enhance solid-state lithium battery performance. The incorporation of LiPO2F2 facilitates the formation of a robust cathode/electrolyte interface composed of LiPxOxF2, LiF, and Li3PO4, significantly improving interfacial stability between the NCM cathode and Li5.5PS4.5Cl1.5

electrolyte (Figure 13c). As a result, the solid-state battery delivers outstanding cycling stability, maintaining 85.5% capacity retention after 600 cycles at 0.5 C (Figure 13d).

In summary, space charge effects in solid-state batteries pose significant challenges due to interfacial rigidity and electrochemical potential mismatches between electrodes and solid electrolytes, leading to ion transport barriers and degraded performance. Recent advancements focus on interfacial engineering strategies to mitigate these effects while enhancing ionic conductivity and stability. Composite electrolytes incorporating dielectric materials or polarized phases effectively suppress space charge regions by homogenizing electric fields and promoting rapid ion transport. Coatings on cathode surfaces, such as ferroelectric or hybrid ionic-conductive layers, reduce interfacial resistance by stabilizing charge transfer pathways and controlling space charge region thickness. Additionally, polymer-based interfacial modifications and additives improve mechanical adhesion and electrochemical compatibility, facilitating uniform ion flux and reducing electron localization. These approaches collectively enhance interfacial kinetics, stabilize longterm cycling, and enable high-voltage operation, underscoring the importance of tailored interfacial design in overcoming fundamental limitations of solid-state battery systems.

4 | Characterization Methodologies on Interfacial Storage

The elucidation of interfacial storage mechanisms and associated phenomena critically relies on state-of-the-art

characterization techniques to resolve the complex interplay of physicochemical interactions and structural evolution at interfaces. These approaches enable multi-scale analysis capabilities spanning atomic-level resolution of interfacial architectures to dynamic interfacial processes accompanying charge/discharge cycling. By integrating complementary characterization platforms, researchers gain insights into atomic arrangements at interfaces, charge transfer kinetics across phase boundaries, and metastable intermediate states governing storage behaviors. Principal methodologies include in situ characterizations that combine temporal resolution with chemical specificity, as well as multimodal techniques correlating structural, electronic, and ionic dynamics. This section provides a structured overview of the advanced experimental techniques essential for deciphering interfacial storage mechanisms, emphasizing their operational principles, spatial-temporal resolution limits, and unique capabilities in probing dynamic interfacial phenomena.

1. Scanning Kelvin Probe Microscopy (SKPM)

SKPM, also referred to surface potential microscopy, serves as a key analytical tool for probing built-in electric fields at heterointerfaces. This technique can measure the contact potential difference between a conductive atomic force microscopy (AFM) tip and the sample surface [87, 88], thereby enabling spatially resolved mapping of surface potentials that reflect localized work function variations and electric field distributions. The resulting high-resolution surface potential mapping provides direct experimental validation of theoretical models describing how interfacial electric fields govern charge transfer, ion diffusion processes, and related interfacial phenomena.

Such insights are particularly valuable for engineering functional interfaces with optimized ion transport kinetics and charge storage efficiency, ultimately improving device performance across EES systems.

Recent applications demonstrate the versatility of SKPM in interfacial characterization. Lu et al. [41] employed SKPM to confirm the presence of built-in electric fields in the TiNbO₅/rGO composite (Figure 14a), revealing an unbalanced surface potential distribution across adjacent nanosheets that enhances both ion diffusion and electron conduction, contributing to an exceptional Na+ storage performance. Complementary in situ TEM analysis further demonstrated uniform Na+ intercalation with minimal volume expansion in the hybrid material. In a parallel study. Kang et al. [63] reported a pronounced differential surface potential shift of 300 mV in the MF-FC electrode during discharge to 0.01 V (Figure 14b), revealing a charge-rich surface distribution with positive polarity compared to the non-fluorinated counterpart (MF-C). This polarization effect from the fluorination enhances Li+ adsorption at the MF-FC surface, thus significantly improving storage capacity. In solid-state battery systems, Masuda et al. [89] employed a cross-sectional SKPM methodology combined with Ar+ milling to map interfacial potential evolution in composite cathodes (Figure 14c). The potential mapping detected a significant increase in potential post-charging, indicating Li⁺ depletion extending into the Li_{1+x}Al_xTi_{2-x}(PO₄)₃ solid electrolyte over micrometer-scale domains. Notably, the observed local potential variations underscored the critical effect of composite electrode microstructure on Li⁺ transport behavior. Moreover, Shi et al. [78] studied the PVBL

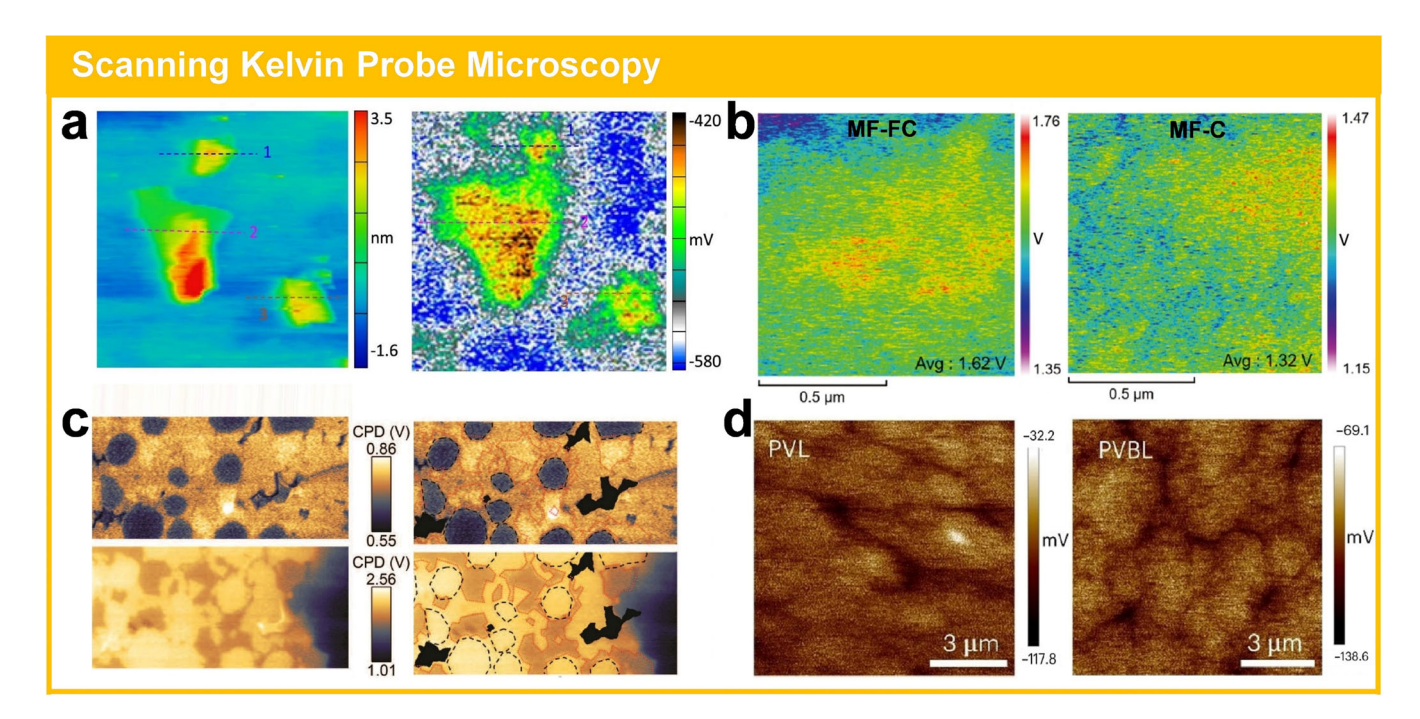


FIGURE 14 | (a) SKPM images of the TiNbO₅/rGO [41]. Reproduced with permission: Copyright 2022, American Chemical Society. (b) SKPM analysis for surface potential differences of the MF-FC and MF-C in fully discharged states [63]. Reproduced with permission: Copyright 2024, WILEY-VCH. (c) Contact potential difference images of the composite cathodes [89]. Reproduced with permission: Copyright 2017, The Royal Society of Chemistry. (d) Interfacial potential images of the PVL and PVBL [78]. Reproduced with permission: Copyright 2023, Springer.

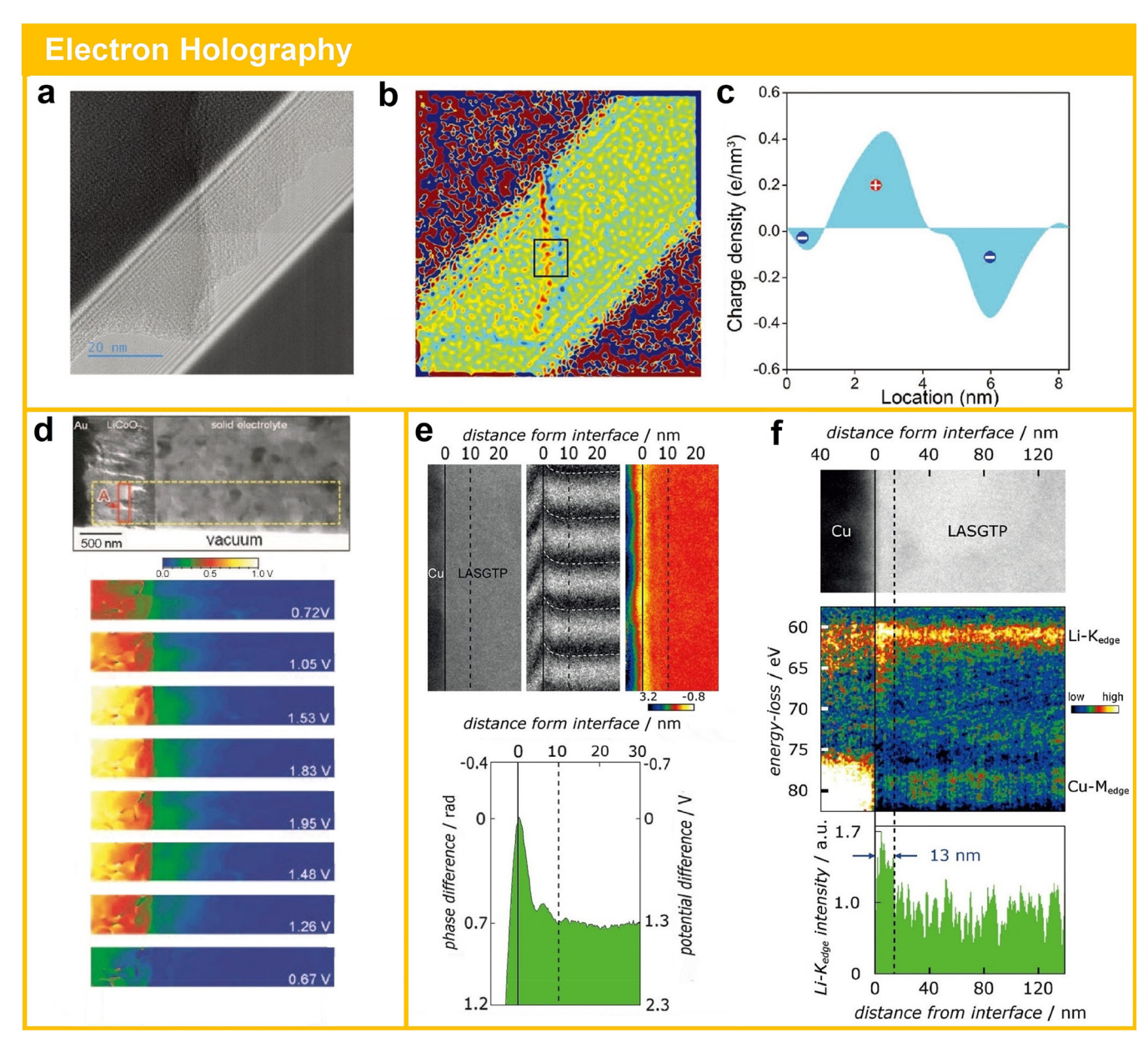


FIGURE 15 | (a) EH image, and (b) the charge density map of the $Ce_{1/3}NbO_3$. (c) Averaged charge density profiles from the black rectangular area in (b) [53]. Reproduced with permission: Copyright 2022, WILEY-VCH. (d) Electric potential distribution at the $LiCoO_2$ /electrolyte interface during charge/discharge [90]. Reproduced with permission: Copyright 2010, WILEY-VCH. (e) Electric potential distribution at the Cu/LASGTP interface obtained from phase-shifting EH. (f) Li^+ distribution at the Cu/LASGTP interface from spatially resolved EELS [91]. Reproduced with permission: Copyright 2019, WILEY-VCH.

solid-state electrolyte using SKPM (Figure 14d), demonstrating that the BTO components effectively reduce interfacial potential barriers between PVDF and BTO-LLTO phases, thereby lowering ion migration energy. This interfacial engineering strategy leverages BTO's dielectric polarization to both dissociate lithium salts and generate built-in electric fields that mitigate space charge effects at polymer-ceramic interfaces.

2. Electron Holography (EH)

EH is an interferometric technique that can measure phase shifts in transmitted electron waves to map electrostatic potentials with sub-nanometer resolution. By converting phase data into electric field distributions, EH visualizes interfacial potential gradients, magnitudes, and spatial variations at the nanoscale. This capability clarifies how space charge regions form and govern ion transport at heterointerfaces. When integrated with electron energyloss spectroscopy (EELS), the EH-EELS platform can simultaneously track dynamic potential distribution, chemical states, and interface structural evolution during electrochemical cycling. This method reveals fundamental correlations between localized potential heterogeneity, metastable charge states, and interfacial degradation, establishing EH as an indispensable tool for elucidating interfacial phenomena in battery systems.

Recent advances have underscored the unique capabilities of EH in probing interfacial storage mechanisms. Liang

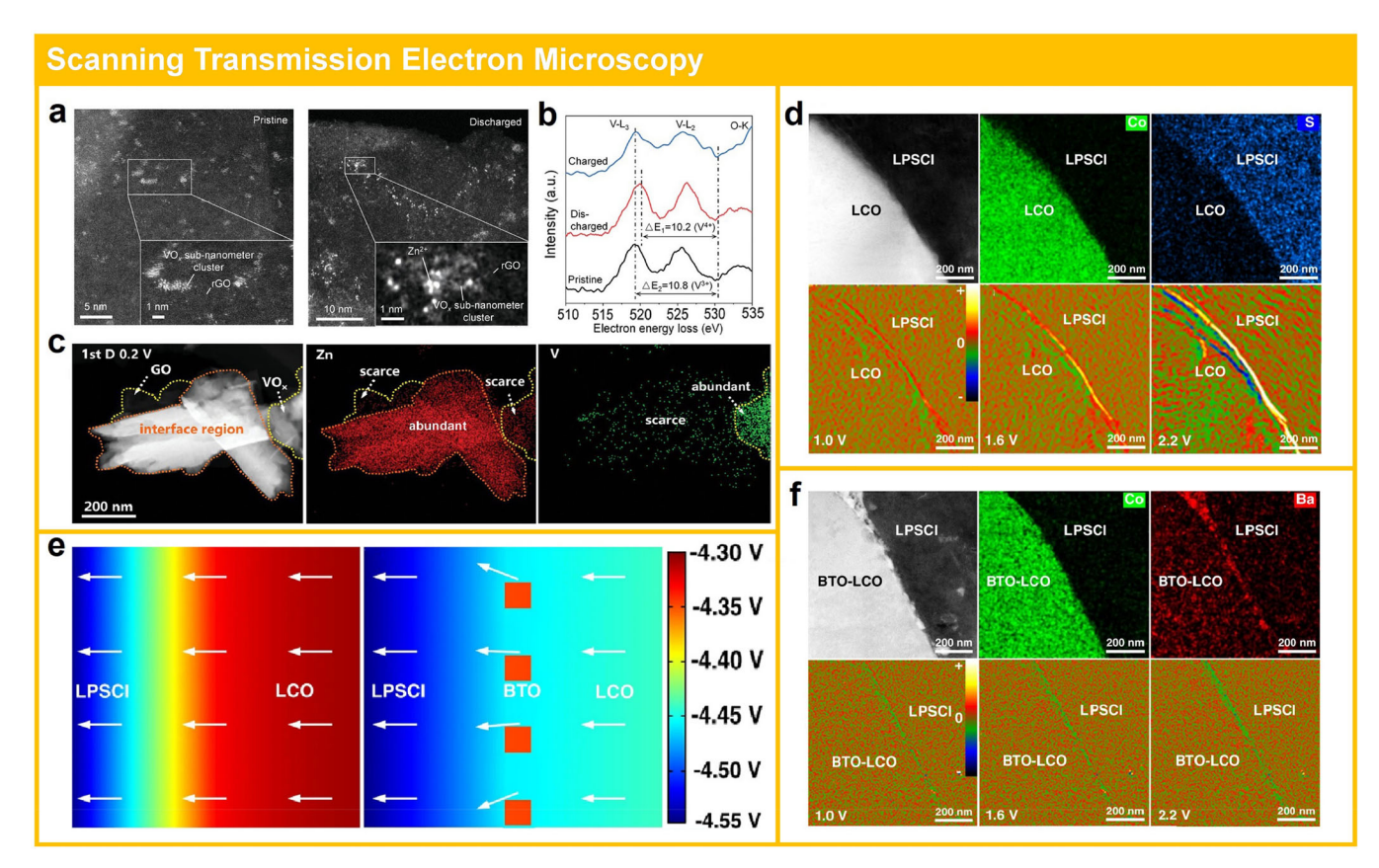


FIGURE 16 | (a) HAADF-STEM images, and (b) EELS spectra of the VO_x/rGO at different charged/discharged states [64]. Reproduced with permission: Copyright 2021, WILEY-VCH. (c) HAADF-STEM image and EDS mappings of the VO_x/GO at the discharged state [35]. Reproduced with permission: Copyright 2024, WILEY-VCH. (d) HAADF-STEM image, EDS mappings, and in situ DPC-STEM images of net-charge-density accumulation at the LCO/LPSCI interface. (e) FEA of the effects of the BTO nanocrystals on the internal electrical field. (f) HAADF-STEM image, EDS mappings, and in situ DPC-STEM images of net-charge-density accumulation at the BTO-LCO/LPSCI interface [92]. Reproduced with permission: Copyright 2020, WILEY-VCH.

et al. [53] employed EH to analyze the surface potential of the Ce_{1/3}NbO₃ electrode, thereby revealing the origin of its extra Na⁺ storage capacity. The charge distribution map derived from EH, along with corresponding line profiles (Figure 15a-c), shows the accumulation of negative surface charge, directly evidencing the formation of interfacial space charge regions, which contributes to additional Na+ storage and enhances rate capability. Yamamoto et al. [90] achieved in situ monitoring of electric potential redistribution in solid-state LIBs during cycling. By applying EH, they quantitatively mapped the 2D potential distribution arising from Li+ migration near the LiCoO2 cathode/electrolyte interface (Figure 15d). Complementary EELS analyses revealed that Li+ extraction during charge induced cobalt oxidation $(Co^{3+} \rightarrow Co^{4+})$ in the cathode material. Similarly, Nomura et al. [91] also resolved the ionic and electric potential profiles in space charge regions the Cu electrode/ $Li_{1+x+y}Al_x(Ti, Ge)_{2-x}Si_yP_{3-y}O_{12}$ (LASGTP) solid electrolyte interface (Figure 15e). EH measurements revealed space charge regions with a defined thickness of 10 nm and a potential barrier of 1.3 V, directly linking Fermi-level misalignment to Li⁺ storage and interfacial band bending. EELS corroborated these findings by spatially resolving Li⁺ enrichment in the space charge regions (Figure 15f). The synergistic EH-EELS provides unprecedented access to nanoscale interfacial phenomena that remain inaccessible through conventional

electrochemical or spectroscopic techniques, offering significant insights for probing and manipulating space charge dynamics at solid-solid interfaces.

3. Scanning Transmission Electron Microscopy (STEM)

STEM serves as an indispensable technique for probing interfacial storage mechanisms at atomic resolution. By integrating HAADF images with EELS or EDS mapping, STEM enables visualization of interfacial atomic arrangements, defects, and element distributions. The advent of in situ differential phase contrast STEM (in situ DPC-STEM) further expands these capabilities by dynamically mapping electric field distributions and charge density gradients under operando conditions. This technique exploits the exceptional sensitivity of DPC to subtle electron beam deflections induced by electromagnetic fields, enabling simultaneous atomic-scale structural imaging and quantitative electric field analysis at heterointerfaces. Such advancements permit real-time tracking of critical interfacial phenomena, including the formation of space charge regions, ion adsorption/desorption kinetics, and field-driven phase transition.

Dai et al. [64] investigated Zn²⁺ storage mechanisms in vanadium-based composites using HAADF-STEM and EELS. Post Zn²⁺ uptake, HAADF-STEM images revealed Zn²⁺ localization adjacent to isolated and irregularly distributed V atoms (Figure 16a). Ex situ EELS demonstrated that pristine

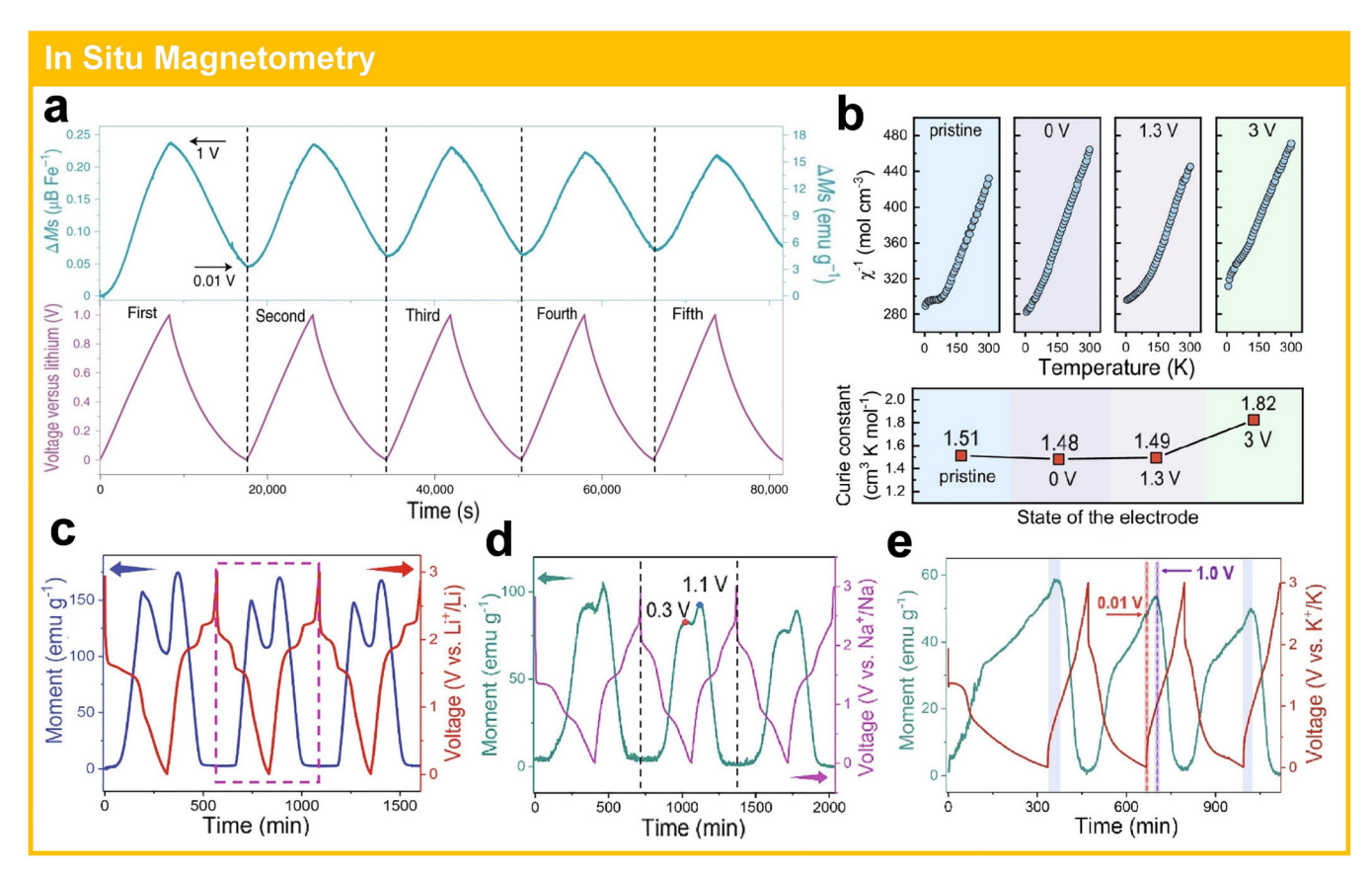


FIGURE 17 | (a) Magnetic responses and charge/discharge curves of the Fe_3O_4/Li systems [93]. Reproduced with permission: Copyright 2021, Springer. (b) Magnetic susceptibility (χ)-temperature curves and the corresponding Curie constants of the Fe/Li_2O [65]. Reproduced with permission: Copyright 2024, Springer. (c-e) Magnetic responses and charge/discharge curves of the $Fe/Se_2/Li$, $Fe/Se_2/Na$, and $Fe/Se_2/K$, respectively [94]. Reproduced with permission: Copyright 2022, Elsevier.

 V^{3+} was oxidized to V^{4+} after Zn^{2+} intercalation and reduced back to V³⁺ upon Zn²⁺ deintercalation (Figure 16b). Notably, this valence change of V opposes conventional bulk or surface storage mechanisms, implicating the interface as the dominant Zn²⁺ storage site. Liu et al. [35] further corroborated the interface-dominated mechanism through ex situ HAADF-STEM and EDS mapping. As shown in Figure 16c, Zn signals were overwhelmingly localized at the interfacial regions, with minimal detection in the bulk domains. Recently, Wang et al. [92] applied in situ DPC-STEM to probe Li+ storage mechanisms at the LiCoO₂/Li₆PS₅Cl (LCO/LPSCl) interfaces. Through direct mapping of net charge density distribution, these authors successfully visualized localized Li⁺ enrichment patterns that exhibited strong correlation with interfacial potential gradients (Figure 16d). Building on these observations, these authors developed a novel dual-modulation strategy of built-in electric field engineering and chemical potential optimization. In situ DPC-STEM and FEA confirmed that coated BaTiO₃ nanoparticles on the LiCoO₂ surface effectively suppress the formation of space charge regions while establishing fast, continuous interfacial Li+ transport pathways (Figure 16e,f).

4. In Situ Magnetometry

In situ magnetometry has emerged as a pivotal technique for probing interfacial storage mechanisms in transition metal-based electrodes, offering unique insights into dynamic spin state evolution, electronic reorganization, and ion migration at heterointerfaces. By correlating real-time magnetic susceptibility and remanence with electrochemical parameters, this technique can decouple interfacial phenomena from bulk processes, enabling quantitative analysis of charge redistribution and phase transition kinetics.

Recent advances in this field have yielded significant breakthroughs in understanding interfacial storage mechanisms across various transition metal compounds. A landmark study by Li et al. [93] demonstrated the power of in situ magnetometry in resolving surface capacitance contributions in transition metal oxide anodes for LIBs. Their study revealed that metallic nanoparticles formed during low-potential discharge host spin-polarized electrons through an interfacial storage mechanism. Magnetic response evolution (Figure 17a) demonstrated that surface capacitance dominates the anomalous capacity in Fe₃O₄/ Li systems, with this phenomenon extending to CoO, NiO, FeF₂, and Fe₂N materials. Moreover, the temperaturedependent magnetic susceptibility analysis provided further mechanistic insights in Fe/Li₂O systems [65]. As shown in Figure 17b, the Curie constant exhibited high stability (~1.5 cm³ K mol⁻¹) from initial state through full discharge (0.01 V) to recharge at 1.3 V. However, a significant increase to 1.82 cm3 K mol-1 when charging to

3 V indicated fundamental changes in the intrinsic magnetic moment and magnetic state of the material. This voltage-dependent behavior strongly supports the predominance of space charge storage mechanism in the 0.01-1.3 V range. Extending this methodology, Li et al. [94] employed in situ magnetometry to investigate interfacial alkali ion storage in FeSe2-based systems. The magnetic profiles revealed M⁺ (Li⁺/Na⁺/K⁺) accumulate at M₂Se phase boundaries while spin-polarized electrons localize in metallic Fe domains, consistent with the jobsharing mechanism. Comparative magnetic analyses revealed that increasing cation ionic radius from Li⁺ through Na⁺ to K⁺ progressively impedes reaction kinetics, resulting in constrained Fe domain formation and reduced space charge storage capacity (Figure 17c-e). Recent work by Chen et al. [60] unveiled a hybrid charge storage mechanism in the Ni@TiO2 heterostructures. Combining in situ magnetometry with thermodynamic simulations, the authors identified a decoupled transport of electrons and ions, enabling conventional intercalation reactions coupled with interfacial space charge storage. The magnetic response demonstrated capacitive characteristics in the potential range of 0-2 V with periodic magnetization variations confirming reversible electrochemical processes. Magnetic characterization was further employed to investigate the Li+ storage behavior of the MF-FC electrode [63]. The magnetic hysteresis loops revealed a significant enhancement in magnetization upon discharging, which can be attributed to the formation of nanosized metallic particles during the reduction process in MF-FC. These metallic nanoparticles facilitate the accumulation of spin-polarized electrons, thereby promoting the adsorption of excess Li+ ions. Upon recharging to 3.0 V, the magnetization decreased markedly but did not return to its initial state, suggesting an irreversible reaction in the MF-FC electrode. The aforementioned in situ magnetometry research establishes interfacial charge storage as a universal mechanism in transition metal-based anodes with accessible high electron density states.

5. In Situ Raman Spectroscopy

In situ Raman spectroscopy, a non-destructive analytical technique, probes molecular vibrational modes via laser-induced inelastic scattering, enabling real-time chemical and structural characterization of heterointerfaces during charge/discharge. By tracking characteristic Raman shifts, this method resolves dynamic interfacial phenomena such as bond reconfiguration, phase transitions, intermediate species formation, and space charge region evolution. These unique capabilities make in situ Raman spectroscopy indispensable for optimizing interfacial architectures in batteries, supercapacitors, and catalytic systems to enhance energy density, longevity, and reaction reversibility.

Liu et al. [95] elucidated the complex multi-physics fields at lithium metal/electrolyte interfaces using in situ Raman spectroscopy. They revealed the formation of an anion depletion layer during lithium deposition, which establishes a space charge region characterized by localized electric fields and interfacial potential gradients. Raman

analysis demonstrated that the magnitude of space charge region is governed by anion mobility, solvation structures, and solvent environment, with anion transport kinetics identified as the dominant factor tuning interfacial polarization. Chen et al. [82] employed in situ Raman spectroscopy to trace space charge region evolution and assess structural stability in the Li₆PS₅Cl solid electrolyte/ LiNbO₃-coated NCM cathode. By correlating Raman peak frequency shifts with applied mechanical pressure, these authors confirmed that the solid electrolyte maintains structural integrity without lattice distortion or irreversible phase transitions under cycling under varied thermal processing conditions (Figure 18a-c), attributed to well-controlled space charge regions. This reversible interfacial evolution ensures stable Li⁺ migration at the cathode interface, highlighting the critical role of space charge region control in preserving interfacial kinetics.

6. Nuclear Magnetic Resonance (NMR)

NMR spectroscopy serves as a powerful noninvasive tool for probing atomic-scale chemical environments, ion transport dynamics, and interfacial structural evolution in battery systems. By analyzing nucleus-specific resonance shifts and spin relaxation times, this technique enables quantitative characterization of ion diffusion kinetics, structures at interfaces, and redistribution mechanisms. Notably, NMR provides unique capabilities in identifying metastable interfacial phases, monitoring the evolution of solid electrolyte interface (SEI) layers, and correlating ion mobility with electrochemical performance. These capabilities provide critical insights for designing interfaces with enhanced ion transport and stability. Zettl et al. [96] revealed through ⁷Li NMR spin fluctuation analysis that LiBH₄/Al₂O₃ heterostructures form percolating networks of fast ionic conduction pathways. The observed accelerated spin dynamics confirmed ultrafast Li⁺ hopping in the LiBH₄/ Al₂O₃ and LiBH₄-LiI/Al₂O₃ composites (Figure 19a), thereby establishing a fundamental link between interfacial architecture and ionic conductivity. Subsequently, Gombotz et al. [97] extended these findings to LiF/TiO₂ composites using conductivity spectroscopy and variabletemperature ⁷Li/¹⁹F NMR line-shape (Figure 19b,c). The LiF/TiO2 interface showed a fourorder-of-magnitude conductivity increase compared to the LiF nanocrystalline, highlighting the critical role of interface engineering.

Li et al. [98] engineered conjugated polymer/oxide electrolyte interfaces (LLZTO@P-DOL) with charge-rich space charge regions via in situ polymerization. Solid-state ⁷Li NMR spectra coupled with computational modeling revealed that optimized space charge configurations not only facilitate Li⁺ transport but also promote inorganic-rich SEI formation on lithium anodes (Figure 19d), enabling uniform lithium deposition. In addition, solid-state NMR analysis of the PVBL electrolyte incorporating BTO-LLTO nanowires revealed that the ⁶Li content in LLTO increased from 13% to 30%, with 17% of the increase attributed to LLTO-mediated transport [78].

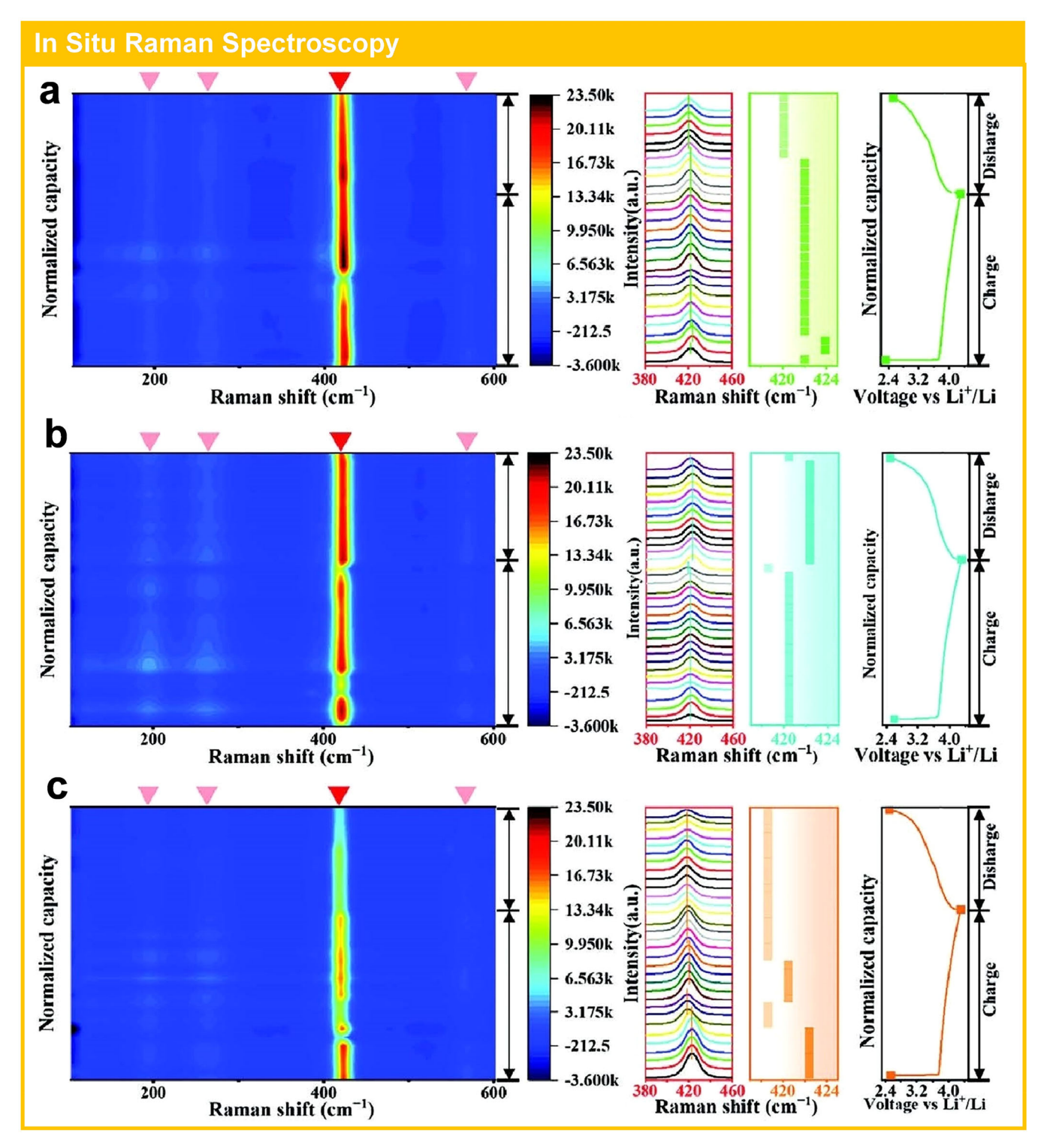


FIGURE 18 | (a-c) In Situ Raman spectra of interfacial evolution in the Li₆PS₅Cl electrolyte/LiNbO₃-coated NCM cathode under varied thermal processing conditions (300, 600, and 850°C, respectively) [82]. Reproduced with permission: Copyright 2024, WILEY-VCH.

These results demonstrated that the BTO-LLTO coupling significantly enhances Li⁺ participation in LLTO conduction pathways, emphasizing the role of BTO in optimizing ion transport. In a systematic investigation of space charge effects, Cheng et al. [99] modulated the $\text{Li}_x\text{V}_2\text{O}_5/\text{Li}_{1.5}\text{Al}_{0.5}\text{Ge}_{1.5}(\text{PO}_3)_4$ (LAGP) interfaces via electrochemical potential control. 2D NMR exchange spectroscopy exhibited the Li⁺ transport activation energy

increased from 0.315 eV (space charge-free interface) to 0.515 eV (modified interface), with reduced exchange current densities directly correlating to space charge-induced interfacial resistance (Figure 20). These findings establish a quantitative relationship between charge distribution in space charge regions and ion migration barriers, which provides guidelines for electrode/electrolyte interface engineering.

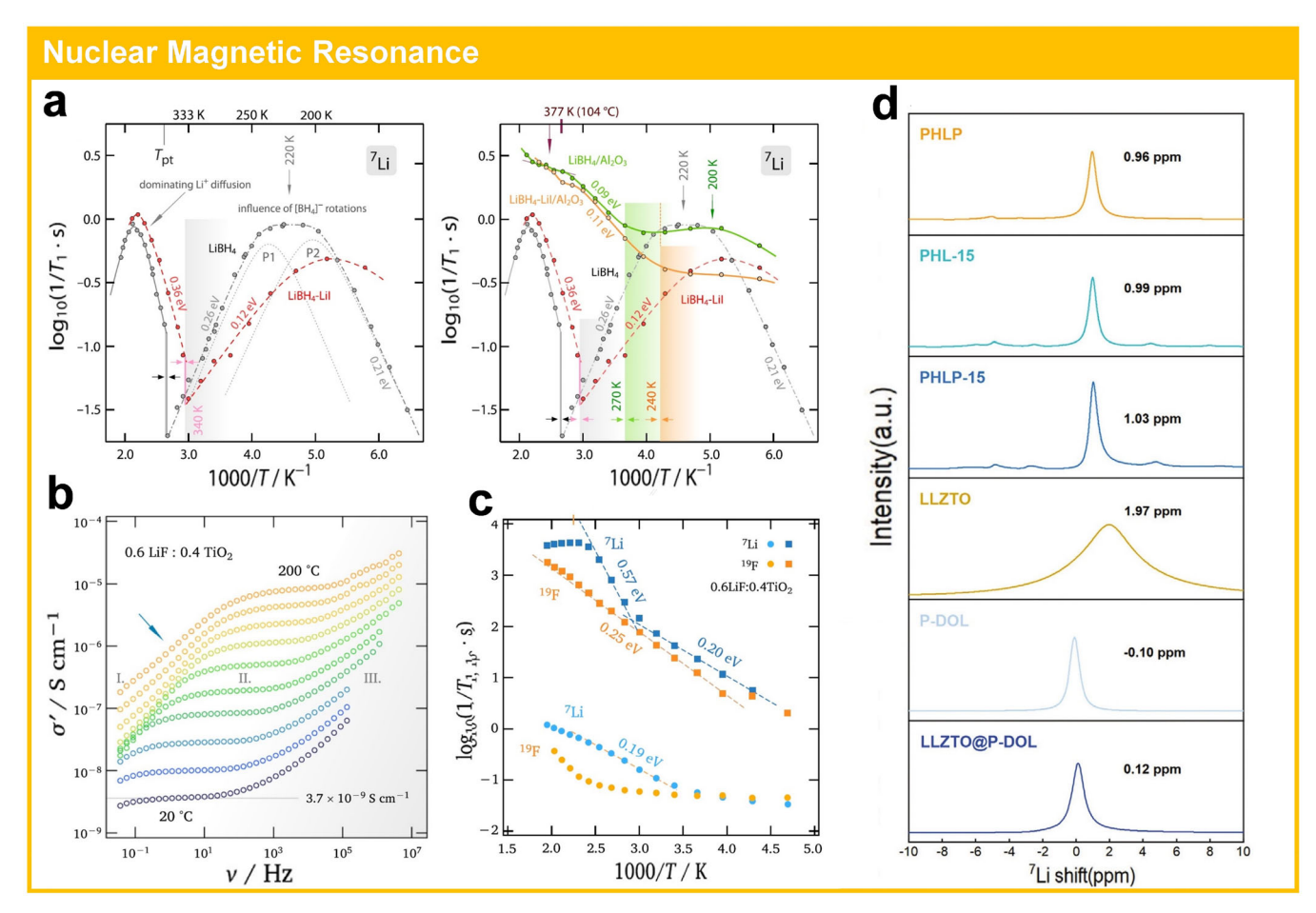


FIGURE 19 | (a) ⁷Li NMR responses of the LiBH₄/Al₂O₃ [96]. Reproduced with permission: Copyright 2022, American Chemical Society. (b) Conductivity isotherms, and (c) variable-temperature ⁷Li/¹⁹F NMR relaxation rates of the LiF/TiO₂ [97]. Reproduced with permission: Copyright 2021, Elsevier. (d) ⁷Li solid-state NMR spectra of the LLZTO@P-DOL [98]. Reproduced with permission: Copyright 2024, WILEY-VCH.

Advanced characterization techniques have enhanced our understanding of interfacial phenomena by enabling direct observation of dynamic processes such as interface structure evolution, space charge formation, spin-polarized electron localization, and metastable phase formation. These tools have demonstrated how engineered interfaces can reduce ion migration barriers, improve storage capacity, and suppress space charge effects. Nevertheless, significant gaps persist between mechanistic understanding and practical application. Current limitations stem from several critical challenges. While modern techniques achieve atomic/ nanoscale resolution, their reliance on idealized or ex situ conditions often obscures the true complexity of operational electrochemical environments. Moreover, establishing clear correlations between atomically resolved interfacial dynamics and macroscopic device performance remains elusive. For example, localized electric fields visualized through SKPM or EH may not accurately reflect bulk-scale ion transport behavior in composite electrodes. Additionally, while each analytical method provides unique insights, no single technique can fully capture the intricate interplay between structural, electronic, and ionic processes at interfaces.

Addressing these challenges requires three key advancements. First, the development of operando multimodal platforms that combine complementary characterization methods to simultaneously monitor structural, electronic, and ionic dynamics under realistic operating conditions. Second, deeper integration of computational approaches with experimental studies to predict interfacial behavior and accelerate materials discovery. Third, implementation of standardized testing protocols that incorporate real-world stressors like high current densities, thermal fluctuations, and mechanical strain to evaluate interfacial stability beyond idealized laboratory conditions. Bridging these fundamental breakthroughs to real-world implementation will require coordinated efforts among materials scientists, electrochemists, process engineers, and industrial partners to establish scalable fabrication processes for tailored heterointerfaces and engineered composite systems with enhanced performance metrics.

5 | Summary and Outlook

Contemporary battery systems have long relied on coupled ionelectron storage in bulk materials, a paradigm inherently limited by sluggish solid-state diffusion kinetics and structural degradation. The emerging interfacial storage mechanisms that spatially decouple charge carrier transfer pathways through

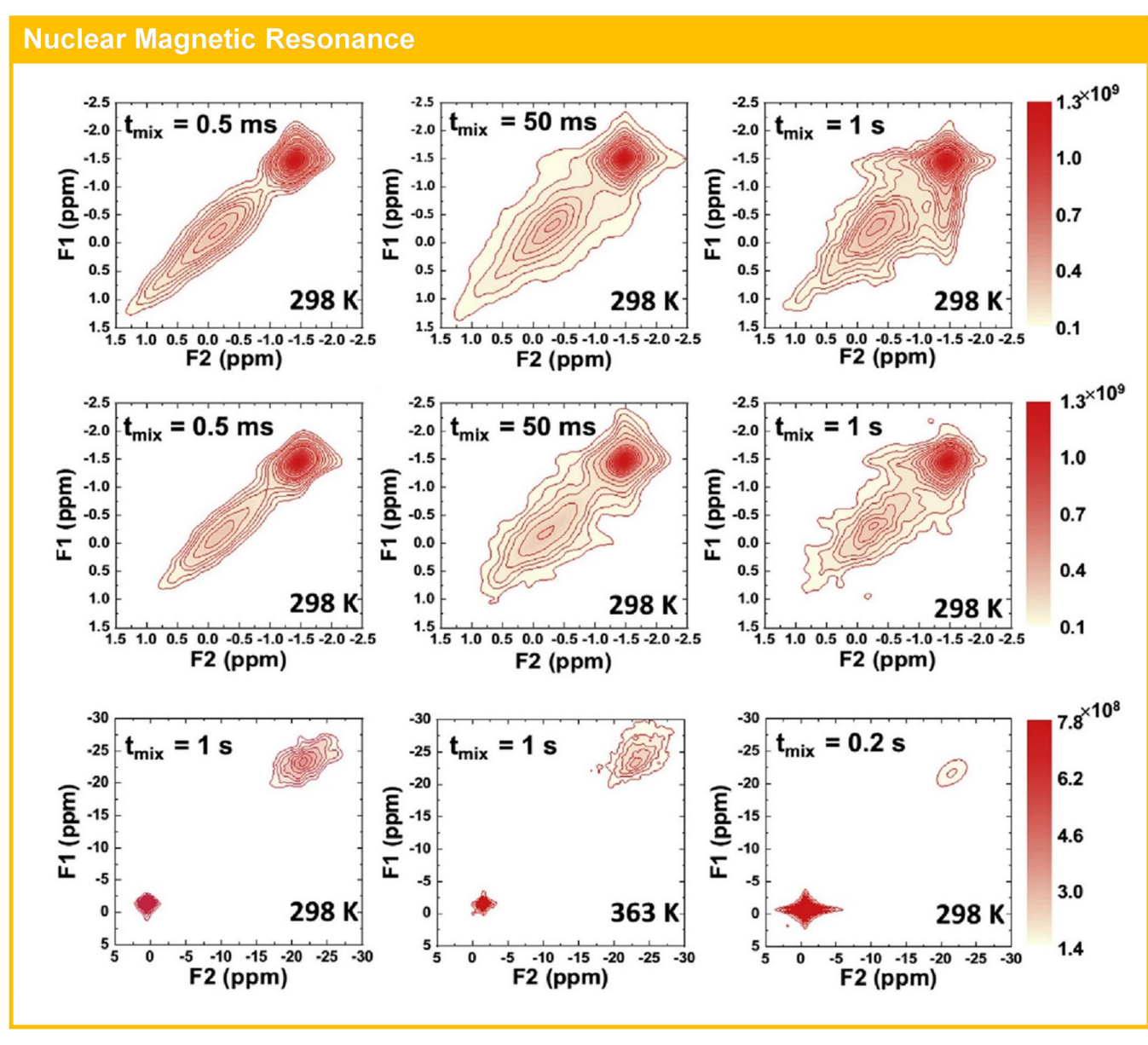


FIGURE 20 | 2D NMR exchange spectra of the Li_xV₂O₅/LAGP [99]. Reproduced with permission: Copyright 2022, Elsevier.

engineered heterointerfaces offer transformative solutions to these challenges. First, interfacial storage overcomes bulk diffusion limitations by confining charge transfer to nanoscale space charge regions. Built-in electric fields at heterointerfaces act as electrostatic pumps, reducing activation barriers for ion migration while directing electrons through low-resistance pathways. Second, by expanding charge storage zones to interfacial regions, interfacial storage unlocks capacity exceeding bulk limitations. Dimensionally optimized nanocomposites demonstrate that the majority of the total capacity originates from interfacial storage. Third, engineered heterointerfaces mitigate mechanical strain and chemical degradation through dynamic buffering effects. Reversible interfacial bonds accommodate volume changes during cycling, while self-healing chemistries suppress particle detachment and dissolution. Additionally, rational interface engineering (e.g., dielectric composites, cathode coatings, polymer modifications) mitigates space charge effects in solid-state batteries, lowering ion transport barriers and enhancing kinetics.

A thorough understanding of interfacial storage mechanisms requires the integration of advanced characterization methodologies. Cutting-edge high-resolution microscopy techniques reveal interfacial structural evolution across atomic to mesoscopic scales, while sophisticated spectroscopic methods elucidate chemical and electronic states at phase boundaries. Emerging approaches like in situ magnetometry enable correlation between magnetic properties and interfacial charge redistribution, complemented by computational modeling that bridges theoretical predictions with experimental results. Together, these methodologies provide a multidimensional analytical framework for elucidating interfacial structural evolution and storage behavior, facilitating mechanism-guided material design.

These advances position interfacial storage as a paradigmshifting strategy for next-generation batteries, effectively bridging the energy-power tradeoff and enabling diverse applications from grid-scale energy storage to high-power electronics. Despite these remarkable breakthroughs, the translation of interfacial storage concepts from laboratory demonstrations to commercial viability faces several critical challenges:

1. Scalable Construction of High-Density Interfaces

Current interfacial storage systems heavily rely on atomic-scale heterointerfaces, which demand precise control over material composition, crystallinity, and topology. However, conventional synthesis methods, such as hydrothermal growth, sol-gel processes, and mechanical mixing, struggle to achieve uniform and high interfacial densities at scale. For example, the fabrication of interface-rich composites involves energy-intensive and low-yield processes, such as melt-quenching and vacuum filtration [64]. The lack of industrially compatible techniques for mass-producing nanocomposites with tailored interface geometries remains a critical bottleneck.

2. Stability of Space Charge Regions

The electrochemical reversibility of interfacial storage hinges on the stability of built-in electric fields and space charge regions. Interfacial charge redistribution can induce electrostatic screening (e.g., counterion accumulation) or mechanical strain (e.g., lattice mismatch) during cycling, leading to field attenuation and capacity fade. For instance, hydrogen-bonding interfaces demonstrate gradual bond dissociation under high-rate cycling, thus necessitating self-repair mechanisms [35]. Ensuring the long-term stability of nanoscale interfaces under extreme conditions remains unresolved.

3. Limited Fundamental Understanding

While advanced characterization tools have uncovered interfacial phenomena, critical knowledge gaps persist. First, most studies capture static "snapshots" of interfaces, neglecting real-time structural and electronic rearrangements during charge/discharge cycling. For example, the interplay between active ions and space charge regions at interfaces is poorly understood. Second, the contribution of bulk phases to interfacial storage is rarely quantified. Ambiguous distinctions between interfacial capacitance and bulk intercalation complicate performance optimization. Third, current strategies are largely empirical, lacking predictive models correlating interface chemistry (e.g., work function mismatch, lattice constants) with performance metrics, which hinders rational interfacial design.

4. Cost and Sustainability

Many high-performance interfacial storage systems rely on scarce or toxic materials, such as MXene, graphene, and 2D transition metal dichalcogenides (TMD). These materials encounter significant scalability challenges due to their intricate synthesis processes and high precursor costs. For example, MXene production typically involves HF etching, raising serious environmental and safety concerns, while the synthesis of rGO demands energy-intensive processing. Furthermore, effective recycling methods for nanocomposites, particularly those with atomic-scale interfacial architectures, remain underdeveloped, posing critical sustainability challenges across their lifecycle.

5. Integration with Existing Infrastructure

Adopting interfacial storage technologies requires compatibility with current battery manufacturing workflows. However, slurry-based electrode fabrication may destroy delicate interfacial architectures, while all-solid-state designs demand new assembly techniques. Furthermore, the low tap density of nanocomposites reduces volumetric energy density, limiting their appeal for portable electronics.

To address these challenges and unlock the full potential of interfacial storage, future research should focus on the following directions:

1. Atomic-Scale Interface Engineering

Precise engineering of interfacial defects (e.g., vacancies, interstitial ions, dislocations) enables effective modulation of space charge regions and built-in electric fields. Advanced techniques like atomic layer deposition and molecular beam epitaxy provide sub-nanometer control over the interface, allowing for atomically tailored interfacial architectures. Carefully engineered heterointerfaces with compositional gradients can homogenize mechanical stress and electric field distributions, thereby enhancing cyclability. Furthermore, the development of stimuliresponsive interfaces could pave the way for adaptive charge storage systems that self-optimize under operational conditions.

2. Advanced Characterization and Modeling

The development of multimodal characterization platforms will be instrumental in obtaining correlated insights into the structural, electronic, and ionic kinetics governing interfacial storage. For example, combining in situ synchrotron X-ray diffraction (XRD) with electrochemical impedance spectroscopy (EIS) enables real-time tracking of phase evolution at heterointerfaces, providing unprecedented mechanistic understanding of interfacial phenomena. To advance rational interfacial design, machine learning-driven approaches, such as training predictive models on interfacial property databases (e.g., work function differences, ionic conductivities), can be leveraged to identify optimal heterointerface configurations, while generative adversarial networks could facilitate the discovery of novel nanocomposites with tailored interfacial properties. Additionally, multiscale simulations will also play a pivotal role in advancing interfacial storage research by bridging ab initio calculations (e.g., DFT for electronic structure analysis) with mesoscale models (e.g., phase-field simulations for ion transport or FEA for stress evolution). The integrated computational framework will be instrumental in elucidating interface-bulk interactions, ultimately providing a theoretical foundation for rational interface design and optimization.

3. Scalable and Sustainable Manufacturing

To enable scalable and sustainable manufacturing of advanced heterointerface materials, several key strategies are emerging. First, green synthesis routes such as biotemplating and solvent-free processes are being developed to replace hazardous chemical-based production methods,

significantly reducing environmental impact. Biotemplating uses biological molecules or microstructures as scaffolds to guide the hierarchical assembly of inorganic/ organic components through biomimetic recognition mechanisms. This approach operates under ambient conditions with molecular precision, thus minimizing energy consumption and achieving atomic-level control over interfacial configurations. Moreover, solvent-free synthesis routes, such as mechanochemical reactions, melt-phase processes, and vapor deposition, completely eliminate the need for solvent media, thereby mitigating solvent toxicity and reducing purification requirements. These approaches not only avoid energy-intensive hightemperature and high-pressure conditions but also prevent the release of volatile organic compounds derived from solvents, resulting in a synergistic reduction in carbon emissions.

Second, self-assembly techniques leveraging interfacial interactions (e.g., van der Waals, hydrogen bonds, and electrostatic) combined with bio-inspired approaches offer energy-efficient pathways for creating ordered nanocomposites at scale. Third, advanced 3D printing technologies [100, 101] such as electrohydrodynamic printing with nanoscale resolution are revolutionizing fabrication by enabling precise control over interface-rich architectures, allowing simultaneous optimization of interfacial density and mechanical properties in hierarchically structured composites.

4. Stability Optimization

Stability optimization of heterointerfaces can be achieved through the integration of self-healing bonds (e.g., hydrogen bonds and covalent bonds) to enable autonomous repair of microcracks or interfacial damage. These bonds undergo reversible dissociation and reformation during cycling, restoring structural integrity without external intervention. Moreover, strain accommodation can be realized using flexible substrates, such as graphene aerogels or carbon nanofibers, which provide mechanical compliance and elasticity to buffer volume changes in composites [102]. These substrates can mitigate interfacial stress concentration and maintain electrical and structural continuity under cyclic loading. The synergy between self-healing bonds and strainadaptive substrates ensures prolonged interfacial stability by addressing both atomic-scale defects and macroscale mechanical mismatches, thereby enhancing durability and performance in dynamic environments.

5. Application-Tailored Systems

Application-tailored systems in heterointerface engineering address diverse operational demands by optimizing structural and electrochemical properties for specific use cases. For high-power applications, fast interface kinetics are prioritized through minimized space charge regions and enhanced charge transfer pathways, enabling rapid energy storage and release. In extreme environments, interfaces are engineered with materials that exhibit thermal resilience at high temperatures or anti-freezing capabilities at low temperatures, ensuring stable electrochemical performance under harsh conditions. For solid-state battery systems, the focus lies on creating ion-conducting interphases

that suppress space charge effects at solid-solid interfaces, facilitating efficient ion transport while maintaining interfacial stability. These tailored interfaces ensure compatibility with distinct application requirements, advancing the adaptability and reliability of EES technologies across varied applications.

6. Circular Economy Integration

Circular economy integration in heterointerface design emphasizes sustainable material use and system recyclability through two key strategies. First, recyclable interfaces can be engineered using reversible bonds or modular architectures, enabling controlled disassembly and component reuse via stimuli-responsive dissociation mechanisms. Second, lifecycle assessment evaluates the environmental impact of interfacial systems across production, operation, and end-of-life stages, thereby informing the selection of low-footprint materials and energy-efficient processes. These approaches collectively minimize resource depletion and waste generation while maintaining electrochemical performance, aligning advanced battery technologies with circular economy principles that prioritize closed-loop material flows and extended system longevity.

In summary, interfacial storage mechanism represents a fundamental paradigm shift in EES systems, offering a pathway to transcend the limitations of conventional bulk-phase materials. By harnessing the unique properties of nanoscale space charge regions, researchers have achieved unprecedented synergies between energy density, power density, and cycle life. However, the transition from laboratory-scale breakthroughs to industrial-scale deployment demands concerted efforts in materials synthesis, characterization, and system integration. Future advancements rely on interdisciplinary cooperation spanning materials science, electrochemistry, and advanced manufacturing. As the field matures, interfacial storage is poised to play a pivotal role in realizing carbon-neutral energy systems, powering everything from electric vehicles to smart grids with unparalleled efficiency and sustainability. The journey from atomic-scale interface engineering to global energy transformation has just begun, and the opportunities are as vast as the challenges are profound.

Author Contributions

Hui Xu: funding acquisition, investigation, methodology, validation, writing – review and editing, and writing – original draft. Daijie Zhang: methodology, writing – review and editing, and writing – original draft. Weijuan Wang: methodology, writing – review and editing, and writing – original draft. Genxi Yu: methodology, writing – review and editing, and writing – original draft. Maiyong Zhu: writing – original draft, writing – review and editing, supervision, conceptualization, and project administration. Yunjian Liu: funding acquisition, writing – original draft, writing – review and editing, supervision, conceptualization, and project administration.

Acknowledgments

These authors would like to thank the financial support from the Natural Science Foundation of Jiangsu Province (BK20200899) and the China Postdoctoral Science Foundation (2020M681502).

Conflicts of Interest

The authors declare no conflicts of interest.

Data Availability Statement

The authors have nothing to report.

References

- 1. Y. Wang, R. Wang, K. Tanaka, et al., "Accelerating the Energy Transition Towards Photovoltaic and Wind in China," *Nature* 619 (2023): 761–767.
- 2. Z. Liu, Z. Deng, G. He, et al., "Challenges and Opportunities for Carbon Neutrality in China," *Nature Reviews Earth & Environment* 3 (2022): 141–155.
- 3. J. Sun, N. Zhai, J. Miao, and H. Sun, "Can Green Finance Effectively Promote the Carbon Emission Reduction in "Local-Neighborhood" Areas?—Empirical Evidence From China," *Agriculture (London)* 12 (2022): 1550.
- 4. A. C. Dillon, "Carbon Nanotubes for Photoconversion and Electrical Energy Storage," *Chemical Reviews* 110 (2010): 6856–6872.
- 5. G. Wang, M. Yu, and X. Feng, "Carbon Materials for Ion-Intercalation Involved Rechargeable Battery Technologies," *Chemical Society Reviews* 50 (2021): 2388–2443.
- 6. D. Zhang, W. Wang, S. Li, X. Shen, and H. Xu, "Design Strategies and Energy Storage Mechanisms of MOF-Based Aqueous Zinc Ion Battery Cathode Materials," *Energy Storage Materials* 69 (2024): 103436.
- 7. Q. Wu, Y. Zhong, R. Chen, et al., "Cu-Ag-C@ Ni₃S₄ With Core Shell Structure and Rose Derived Carbon Electrode Materials: An Environmentally Friendly Supercapacitor With High Energy and Power Density," *Industrial Crops and Products* 222 (2024): 119676.
- 8. X. Wang, Y. Pan, X. Wang, et al., "High Performance Hybrid Supercapacitors Assembled With Multi-Cavity Nickel Cobalt Sulfide Hollow Microspheres as Cathode and Porous Typha-Derived Carbon as Anode," *Industrial Crops and Products* 189 (2022): 115863.
- 9. D. Zhang and H. Xu, "Nickel Modified TiO_2/C Nanodisks With Defective and Near-Amorphous Structure for High-Performance Sodium-Ion Batteries," *Battery Energy* 3 (2024): 20230032.
- 10. M. D. Slater, D. Kim, E. Lee, and C. S. Johnson, "Sodium-Ion Batteries," *Advanced Functional Materials* 23 (2013): 947–958.
- 11. J. Wei, P. Zhang, J. Sun, et al., "Advanced Electrolytes for High-Performance Aqueous Zinc-Ion Batteries," *Chemical Society Reviews* 53 (2024): 10335–10369.
- 12. W. Wang, D. Liu, Y. Jiang, et al., "Mechanism Enhancement of V_3O_7/V_6O_{13} Heterostructures to Achieve High-Performance Aqueous Zn-Ion Batteries," *Chemical Engineering Journal* 463 (2023): 142309.
- 13. X. Xu, F. Xiong, J. Meng, et al., "Vanadium-Based Nanomaterials: A Promising Family for Emerging Metal-Ion Batteries," *Advanced Functional Materials* 30 (2020): 1904398.
- 14. Y. Zhang, Q. Li, W. Feng, et al., "Valence Engineering via Polyoxometalate-Induced on Vanadium Centers for Efficient Aqueous Zinc-Ion Batteries," *Angewandte Chemie International Edition* 64 (2025): 202501728.
- 15. Y. Liu, S. P. Jiang, and Z. Shao, "Intercalation Pseudocapacitance in Electrochemical Energy Storage: Recent Advances in Fundamental Understanding and Materials Development," *Materials Today Advances* 7 (2020): 100072.
- 16. C. C. Chen and J. Maier, "Decoupling Electron and Ion Storage and the Path From Interfacial Storage to Artificial Electrodes," *Nature Energy* 3 (2018): 102–108.

- 17. C. C. Chen, L. Fu, and J. Maier, "Synergistic, Ultrafast Mass Storage and Removal in Artificial Mixed Conductors," *Nature* 536 (2016): 159–164.
- 18. J. Maier, "Thermodynamics of Electrochemical Lithium Storage," Angewandte Chemie International Edition 52 (2013): 4998–5026.
- 19. J. Zhang, J. Zhang, H. Wang, et al., "Solid-Solid Interfacial Charge Storage of Prussian Blue/rGO Mixed-Conductor Cathode for High-Power Na Ion Batteries," *ACS Energy Letters* 7 (2022): 4472–4482.
- 20. R. Usiskin and J. Maier, "Interfacial Effects in Lithium and Sodium Batteries," *Advanced Energy Materials* 11 (2021): 2001455.
- 21. J. Maier, "Mass Storage in Space Charge Regions of Nano-Sized Systems (Nano-Ionics. Part V)," Faraday Discussions 134 (2007): 51–66.
- 22. H. Wang, J. Zhu, Y. Su, Z. Gong, and Y. Yang, "Interfacial Compatibility Issues in Rechargeable Solid-State Lithium Metal Batteries: A Review," *Science China Chemistry* 64 (2021): 879–898.
- 23. Q. Zhang, Y. Kong, K. Gao, et al., "Research Progress on Space Charge Layer Effect in Lithium-Ion Solid-State Battery," *Science China: Technological Sciences* 65 (2022): 2246–2258.
- 24. M. Bärtsch and M. Niederberger, "The Role of Interfaces in Heterostructures," *ChemPlusChem* 82 (2017): 42–59.
- 25. Z. Chen, T. Ma, W. Wei, W. Y. Wong, C. Zhao, and B. J. Ni, "Work Function-Guided Electrocatalyst Design," *Advanced Materials* 36 (2024): 2401568.
- 26. C. C. Chen and J. Maier, "Space Charge Storage in Composites: Thermodynamics," *Physical Chemistry Chemical Physics* 19 (2017): 6379–6396.
- 27. C. C. Chen, E. Navickas, J. Fleig, and J. Maier, "Kinetics of Space Charge Storage in Composites," *Advanced Functional Materials* 28 (2018): 1705999.
- 28. Z. Gu, J. Ma, F. Zhu, et al., "Atomic-Scale Study Clarifying the Role of Space-Charge Layers in A Li-Ion-Conducting Solid Electrolyte," *Nature Communications* 14 (2023): 1632.
- 29. M. A. Frechero, M. Rocci, G. Sánchez-Santolino, et al., "Paving the way to Nanoionics: Atomic Origin of Barriers for Ionic Transport Through Interfaces," *Scientific Reports* 5 (2015): 17229.
- 30. W. Li, Q. Song, M. Li, et al., "Chemical Heterointerface Engineering on Hybrid Electrode Materials for Electrochemical Energy Storage," *Small Methods* 5 (2021): 2100444.
- 31. J. Li, H. Yang, J. Wu, S. Sun, T. Zhai, and H. Xia, "Harnessing the Defects at Hetero-Interface of Transition Metal Compounds for Advanced Charge Storage: A Review," *Small Structures* 3 (2022): 2200022.
- 32. H. L. Tuller and S. R. Bishop, "Point Defects in Oxides: Tailoring Materials Through Defect Engineering," *Annual Review of Materials Research* 41 (2011): 369–398.
- 33. S. J. Kim, J. Y. Koo, T. Mun, M. Choi, and W. Lee, "Tailoring Defect Chemistry at Interfaces for Promoted Oxygen Reduction Reaction Kinetics," *Journal of Materials Chemistry A* 8 (2020): 23313–23322.
- 34. T. Liu, L. Yu, J. Liu, et al., "Ultrastable Cathodes Enabled by Compositional and Structural Dual-Gradient Design," *Nature Energy* 9 (2024): 1252–1263.
- 35. D. Liu, W. Wang, S. Li, X. Shen, H. Xie, and H. Xu, "Interface-Dominated Zn²⁺ Storage in Hydrogen-Bonding Interfaces," *Advanced Functional Materials* 18 (2024): 2402584.
- 36. Y. Li, Y. Lu, P. Adelhelm, M. M. Titirici, and Y. S. Hu, "Intercalation Chemistry of Graphite: Alkali Metal Ions and Beyond," *Chemical Society Reviews* 48 (2019): 4655–4687.
- 37. V. A. Nikitina, S. Y. Vassiliev, and K. J. Stevenson, "Metal-Ion Coupled Electron Transfer Kinetics in Intercalation-Based Transition Metal Oxides," *Advanced Energy Materials* 10 (2020): 1903933.

- 38. Y. Zheng, T. Zhou, X. Zhao, et al., "Atomic Interface Engineering and Electric-Field Effect in Ultrathin $\rm Bi_2MoO_6$ Nanosheets for Superior Lithium Ion Storage," *Advanced Materials* 29 (2017): 1700396.
- 39. L. Fang, Z. Lan, W. Guan, et al., "Hetero-Interface Constructs Ion Reservoir to Enhance Conversion Reaction Kinetics for Sodium/Lithium Storage," *Energy Storage Materials* 18 (2019): 107–113.
- 40. S. Yin, X. Zhang, X. Huang, F. Zhou, Y. Wang, and G. Wen, "SnO/SnO₂ Heterojunction Nanoparticles Anchored on Graphene Nanosheets for Lithium Storage," *ACS Applied Nano Materials* 7 (2024): 14419–14430.
- 41. X. Lu, Y. Shi, D. Tang, et al., "Accelerated Ionic and Charge Transfer Through Atomic Interfacial Electric Fields for Superior Sodium Storage," *ACS Nano* 16 (2022): 4775–4785.
- 42. P. Liang, T. Xu, K. Zhu, et al., "Heterogeneous Interface-Boosted Zinc Storage of $H_2V_3O_8$ Nanowire/ $Ti_3C_2T_x$ Mxene Composite Toward High-Rate and Long Cycle Lifespan Aqueous Zinc-Ion Batteries," *Energy Storage Materials* 50 (2022): 63–74.
- 43. F. Li, H. Sheng, Y. Qi, et al., "MoS₂/ZnS Heterostructure Cathode With Intralayer Regulation for Eco-Friendly, Degradable Zinc-Ion Batteries," *Chemical Engineering Journal* 502 (2024): 157850.
- 44. Y. Xiao, Q. Gu, H. Li, M. Li, and Y. Wang, "Design of a Cationic Accelerator Enabling Ultrafast Ion Diffusion Kinetics in Aqueous Zinc-Ion Batteries," *Journal of Energy Chemistry* 100 (2025): 377–384.
- 45. S. Kim, H. Jung, W. G. Lim, et al., "A Versatile Strategy for Achieving Fast-Charging Batteries via Interfacial Engineering: Pseudocapacitive Potassium Storage Without Nanostructuring," *Small* 18 (2022): 2202798.
- 46. X. Zhang, X. He, S. Yin, et al., "Rational Design of Space-Confined Mn-Based Heterostructures With Synergistic Interfacial Charge Transport and Structural Integrity for Lithium Storage," *Inorganic Chemistry* 61 (2022): 8366–8378.
- 47. C. Li, X. Yao, L. Luo, et al., "2D-2D Nanosheets for Efficient Zinc-Ion Batteries: Synthesis of Interface-Enriched MoS₂ on VN Hybrid Nanosheets," *Journal of Energy Storage* 98 (2024): 113193.
- 48. Y. Chen, X. Chen, K. Zhang, Y. Liu, G. Han, and G. Xu, "Organic-Inorganic Hybrid Cathode Enabled by In-Situ Interface Polymerization Engineering Boosts Zn²⁺ Desolvation in Aqueous Zinc-Ion Batteries," *Journal of Colloid and Interface Science* 681 (2025): 35–43.
- 49. N. Jiang, Y. Zhang, Y. Zhao, et al., "Spontaneous Redox Reaction-Mediated Interfacial Charge Transfer in Titanium Dioxide/Graphene Oxide Nanoanodes for Rapid and Durable Lithium Storage," *Dalton Transactions* 53 (2024): 3348–3355.
- 50. M. Yang, Y. Wang, D. Ma, et al., "Unlocking the Interfacial Adsorption-Intercalation Pseudocapacitive Storage Limit to Enabling All-Climate, High Energy/Power Density and Durable Zn-Ion Batteries," *Angewandte Chemie International Edition* 62 (2023): 202304400.
- 51. J. Li, Q. Guan, Y. Li, et al., "Electron Pump' of Homo-Interface Enhancing D/P-Band Center Proximity for Zinc Storage," *Chemical Engineering Journal* 483 (2024): 149205.
- 52. Z. Lv, Y. Tan, Y. Kang, et al., "Non-Desolvation Zn^{2+} Storage Mechanism Enables MoS_2 Anode With Enhanced Interfacial Charge-Transfer Kinetics for Low Temperature Zinc-Ion Batteries," *Science China Chemistry* 66 (2023): 1537–1548.
- 53. G. Liang, L. Yang, X. Xiong, et al., "Interfacial Space Charge Enhanced Sodium Storage in a Zero-Strain Cerium Niobite Perovskite Anode," *Advanced Functional Materials* 32 (2022): 2206129.
- 54. H. Yang, W. Kong, J. Yin, et al., "Coupled Artificial Mixed Conductor Interfaces Boosts Excess Li-Storage Capability and Ultra-Long Cycle Durability in Si Composite," *Surfaces and Interfaces* 26 (2021): 101435.

- 55. C. Ma, Y. Hou, K. Jiang, et al., "In Situ Cross-Linking Construction of 3D Mesoporous Bimetallic Phosphide-in-Carbon Superstructure With Atomic Interface Toward Enhanced Sodium Ion Storage Performance," *Chemical Engineering Journal* 413 (2021): 127449.
- 56. Z. Yan, Z. Sun, H. Liu, et al., "Heterogeneous Interface in Hollow Ferroferric Oxide/Iron Phosphide@Carbon Spheres Towards Enhanced Li Storage." *Journal of Colloid and Interface Science* 617 (2022): 442–453.
- 57. Z. Liu, J. Huang, B. Liu, et al., "Constructing Enhanced Pseudocapacitive Li⁺ Intercalation via Multiple Ionically Bonded Interfaces Toward Advanced Lithium Storage," *Energy Storage Materials* 24 (2020): 138–146.
- 58. B. Zhao, Q. Liu, Y. Chen, Q. Liu, Q. Yu, and H. B. Wu, "Interface-Induced Pseudocapacitance in Nonporous Heterogeneous Particles for High Volumetric Sodium Storage," *Advanced Functional Materials* 30 (2020): 2002019.
- 59. Y. Lin, H. Kang, M. Liang, et al., "Hybrid Nanostructured MnO_2 Nanowire/Graphdiyne With Enhanced Lithium-Ion Performance Promoting by Interfacial Storage," *Applied Surface Science* 526 (2020): 146457.
- 60. L. Chen, H. Yu, D. Zhu, et al., "Designing Electron/Ion Dual-Phase Conductor $Ni@TiO_2$ for High-Performance Lithium-Ion Storage: Combining Insertion and Space Charge Mechanism," *Applied Physics Letters* 124 (2024): 133901.
- 61. Y. Zhang, Y. Xu, Y. Ji, et al., "Constructing Radially Oriented Macroporous Spheres With Central Cavities as Ultrastable Lithium-Ion Battery Anodes," *Energy Storage Materials* 17 (2019): 242–252.
- 62. L. Zhao, T. Wang, F. Li, et al., "Auxiliary Thermodynamic Analysis Support Capturing the Differences in Nanostructured FeVO₄·nH₂O Electrodes Between Lithium and Sodium Ions Storage Mechanism," *Chemical Engineering Journal* 452 (2023): 139310.
- 63. S. K. Kang, M. Kim, G. H. Park, J. Ji, S. Hong, and W. B. Kim, "A Charge Confinement Strategy for Boosting Interfacial Space Charge Storage in Manganese Ferrites Enabled by Highly Polarized Fluorinated-Interfacial Layer for High-Energy-Density and Ultrafast Rechargeable Lithium-Ion Batteries," *Advanced Functional Materials* 35 (2025): 2408986.
- 64. Y. Dai, X. Liao, R. Yu, et al., "Quicker and More Zn²⁺ Storage Predominantly From the Interface," *Advanced Materials* 33 (2021): 2100359.
- 65. L. Zhao, T. Wang, F. Zuo, et al., "A Fast-Charging/Discharging and Long-Term Stable Artificial Electrode Enabled by Space Charge Storage Mechanism," *Nature Communications* 15 (2024): 3778.
- 66. D. Zhang, W. Wang, J. Lu, S. Ji, and H. Xu, "A New TiO₂-Based Cathode Material With Interface-Dominated Storage Mechanism for Aqueous Zinc-Ion Batteries," *Small* 21 (2025): 2409304.
- 67. C. Zhao, Y. Li, W. Zhang, et al., "Heterointerface Engineering for Enhancing the Electrochemical Performance of Solid Oxide Cells," *Energy & Environmental Science* 13 (2020): 53–85.
- 68. L. S. de Vasconcelos, R. Xu, Z. Xu, et al., "Chemomechanics of Rechargeable Batteries: Status, Theories, and Perspectives," *Chemical Reviews* 122 (2022): 13043–13107.
- 69. X. Q. Zhou, Xiong, J. Peng, et al., "Tailored Engineering on the Interface Between Lithium Metal Anode and Solid-State Electrolytes," *Energy & Environmental Materials* 8 (2025): 12831.
- 70. T. Qin, X. Zhao, Y. Sui, et al., "Heterointerfaces: Unlocking Superior Capacity and Rapid Mass Transfer Dynamics in Energy Storage Electrodes," *Advanced Materials* 36 (2024): 2402644.
- 71. R. Narayan, C. Laberty-Robert, J. Pelta, J. M. Tarascon, and R. Dominko, "Self-Healing: An Emerging Technology for Next-Generation Smart Batteries," *Advanced Energy Materials* 12 (2022): 2102652.

- 72. H. Wang, P. Wang, Y. Feng, et al., "Recent Advances on Self-Healing Materials and Batteries." *ChemElectroChem* 6 (2019): 1605–1622.
- 73. Y. Li, Z. Yuan, D. Li, et al., "Multi-Interface Combination of Bimetallic Selenide and $V_4C_3T_X$ Mxene for High-Rate and Ultrastable Sodium Storage Devices," *ACS Nano* 18 (2024): 4733–4745.
- 74. H. Liu, L. Jiang, B. Cao, et al., "Van Der Waals Interaction-Driven Self-Assembly of $\rm V_2O_5$ Nanoplates and Mxene for High-Performing Zinc-Ion Batteries by Suppressing Vanadium Dissolution," *ACS Nano* 16 (2022): 14539–14548.
- 75. G. Q. Yuan, X. Wei, Y. C. Su, et al., "Enhancing $\rm Zn^{2+}$ Storage Performance by Constructing the Interfaces Between $\rm VO_2$ and $\rm Co-N-C$ Layers," Small 20 (2024): 2308851.
- 76. F. Yuan, C. Qi, W. Bao, et al., "Asymmetric Orbital Hybridization at the Mxene–VO_{2-x} Interface Stabilizes Oxygen Vacancies for Enhanced Reversibility in Aqueous Zinc-Ion Batteries," *Energy & Environmental Science* 18 (2025): 367–377.
- 77. B. Xiao, J. Chen, C. Hu, et al., "2D Dynamic Heterogeneous Interface Coupling Endowing Extra Zn²⁺ Storage," *Advanced Functional Materials* 33 (2023): 2211679.
- 78. P. Shi, J. Ma, M. Liu, et al., "A Dielectric Electrolyte Composite With High Lithium-Ion Conductivity for High-Voltage Solid-State Lithium Metal Batteries," *Nature Nanotechnology* 18 (2023): 602–610.
- 79. X. Ma, S. Ge, S. Chen, et al., "Constructing a Dielectric Fluorinated Solid Electrolyte for Practically Operated All-Solid-State Lithium-Metal Batteries," *ACS Nano* 19 (2025): 9367–9377.
- 80. G. Xiao, K. Yang, Y. Qiu, et al., "Dielectric-Tailored Space Charge Layer and Ion Coordination Structure for High-Voltage Polymer All-Solid-State Lithium Batteries," *Advanced Materials* 37 (2025): 2415411.
- 81. W. Li, S. Zhang, W. Zheng, et al., "Self-Polarized Organic-Inorganic Hybrid Ferroelectric Cathode Coatings Assisted High Performance All-Solid-State Lithium Battery," *Advanced Functional Materials* 33 (2023): 2300791.
- 82. Y. Chen, L. Huang, D. Zhou, et al., "Elucidating and Minimizing the Space-Charge Layer Effect Between NCM Cathode and $\text{Li}_6\text{PS}_5\text{Cl}$ for Sulfide-Based Solid-State Lithium Batteries," *Advanced Energy Materials* 14 (2024): 2304443.
- 83. H. Liu, Y. Wang, L. Chen, H. Li, and F. Wu, "High-Capacity, Long-Life Sulfide All-Solid-State Batteries With Single-Crystal Ni-Rich Layered Oxide Cathodes," *Advanced Functional Materials* 34 (2024): 2315701.
- 84. G. Liu, N. Cao, L. Zeng, et al., "Sulfide All-Solid-State Battery With Ultrahigh Nickel Layered Oxide Cathode and Capacity," *Small* 21 (2025): 2501224.
- 85. C. Shen, W. Feng, Y. Yu, et al., "In Situ Polymerization Inhibiting Electron Localization in Hybrid Electrolyte for Room-Temperature Solid-State Lithium Metal Batteries," *Advanced Energy Materials* 14 (2024): 2304511.
- 86. Z. Wu, L. Du, T. Yang, et al., "Lithium Difluorophosphate Additive Engineering Enabling Stable Cathodic Interface for High-Performance Sulfide-Based All-Solid-State Lithium Battery," *Energy & Environmental Materials* 8 (2025): 12871.
- 87. Y. Qi, M. W. Swift, E. J. Fuller, and A. A. Talin, "Interface Potentials Inside Solid-State Batteries: Origins and Implications," *MRS Bulletin* 48 (2023): 1239–1246.
- 88. S. Su, J. Zhao, and T. H. Ly, "Scanning Probe Microscopies for Characterizations of 2D Materials," *Small Methods* 8 (2024): 2400211.
- 89. H. Masuda, N. Ishida, Y. Ogata, D. Ito, and D. Fujita, "Internal Potential Mapping of Charged Solid-State-Lithium Ion Batteries Using in Situ Kelvin Probe Force Microscopy," *Nanoscale* 9 (2017): 893–898.
- 90. K. Yamamoto, Y. Iriyama, T. Asaka, et al., "Dynamic Visualization of the Electric Potential in an All-Solid-State Rechargeable Lithium

- Battery," Angewandte Chemie International Edition 49 (2010): 4414–4417.
- 91. Y. Nomura, K. Yamamoto, T. Hirayama, S. Ouchi, E. Igaki, and K. Saitoh, "Direct Observation of a Li-Ionic Space-Charge Layer Formed at an Electrode/Solid-Electrolyte Interface," *Angewandte Chemie* 131 (2019): 5346–5350.
- 92. L. Wang, R. Xie, B. Chen, et al., "In-Situ Visualization of the Space-Charge-Layer Effect on Interfacial Lithium-Ion Transport in All-Solid-State Batteries," *Nature Communications* 11 (2020): 5889.
- 93. Q. Li, H. Li, Q. Xia, et al., "Extra Storage Capacity in Transition Metal Oxide Lithium-Ion Batteries Revealed by in Situ Magnetometry," *Nature Materials* 20 (2021): 76–83.
- 94. X. Li, J. Su, Z. Li, et al., "Revealing Interfacial Space Charge Storage of Li⁺/Na⁺/K⁺ by Operando Magnetometry," *Science Bulletin* 67 (2022): 1145–1153.
- 95. J. Liu, H. Hua, J. Lin, et al, "Optimizing Interface Concentration and Electric Fields for Enhanced Lithium Deposition Behavior in Lithium Metal Anodes," *Energy & Environmental Science* 17 (2024): 5962–5993.
- 96. R. Zettl, K. Hogrefe, B. Gadermaier, et al., "Conductor-Insulator Interfaces in Solid Electrolytes: A Design Strategy to Enhance Li-Ion Dynamics in Nanoconfined LiBH₄/Al₂O₃," *Journal of Physical Chemistry C* 125 (2021): 15052–15060.
- 97. M. Gombotz, K. P. Pree, V. Pregartner, et al., "Insulator: Conductor Interfacial Regions—Li Ion Dynamics in the Nanocrystalline Dispersed Ionic Conductor LiF: TiO₂," *Solid State Ionics* 369 (2021): 115726.
- 98. J. Li, J. Chen, X. Xu, et al., "Enhanced Interphase Ion Transport via Charge-Rich Space Charge Layers for Ultra-Stable Solid-State Lithium Metal Batteries," *Advanced Energy Materials* 15 (2025): 2402746.
- 99. Z. Cheng, M. Liu, S. Ganapathy, et al., "Revealing the Impact of Space-Charge Layers on the Li-Ion Transport in All-Solid-State Batteries," *Joule* 4 (2020): 1311–1323.
- 100. H. Zhou, G. Zhu, S. Dong, et al., "Ethanol-Induced Ni²⁺-Intercalated Cobalt Organic Frameworks on Vanadium Pentoxide for Synergistically Enhancing the Performance of 3D-Printed Micro-Supercapacitors," *Advanced Materials* 35 (2023): 2211523.
- 101. H. Zhou, S. Gu, Y. Lu, et al., "Stabilizing Ni²⁺ in Hollow Nano MOF/Polymetallic Phosphides Composites for Enhanced Electrochemical Performance in 3D-Printed Micro-Supercapacitors," *Advanced Materials* 36 (2024): 2401856.
- 102. S. Zhang, Y. Li, X. Zhuang, et al., "Nano-Metal-Organic Frameworks Isolated in Mesoporous Structures," *Advanced Materials* 37 (2025): 2418344.